1 Kinetics of Phase Transitions

Sanjay Puri

CONTENTS

1.1 Introduction 2
1.2 Phase Diagrams of Two-Component Mixtures 5
1.2.1 Ising Model and Its Applications 5
1.2.2 Phase Diagrams in the Mean-Field Approximation 6
1.3 Kinetic Ising Models 9
1.3.1 Introduction 9
1.3.2 The Spin-Flip Glauber Model 10
1.3.2.1 Mean-Field Approximation 13
1.3.3 The Spin-Exchange Kawasaki Model 14
1.3.3.1 Mean-Field Approximation 18
1.4 Domain Growth in Systems with Nonconserved Kinetics 20
1.4.1 Case with Scalar Order Parameter 20
1.4.1.1 Static Interfaces or Kinks 23
1.4.1.2 Equation of Motion for Interfaces and Growth Laws 25
1.4.1.3 Correlation Function and Structure Factor 27
1.4.1.4 Short-Distance Singularities and Porod's Law 28
1.4.1.5 Ohta–Jasnow–Kawasaki Theory 31
1.4.1.6 Implications of the OJK Function 36
1.4.1.7 Kawasaki–Yalabik–Gunton Theory 40
1.4.2 Case with Vector Order Parameter 42
1.4.2.1 Generalized Porod's Law 43
1.4.2.2 Bray–Puri–Toyoki Theory 44
1.5 Domain Growth in Systems with Conserved Kinetics 45
1.5.1 Segregation in Binary Alloys 47
1.5.2 Segregation in Binary Fluid Mixtures 52
1.5.2.1 Dimensional Form of Model H 52
1.5.2.2 Domain Growth Laws in Binary Fluids 54
1.6 Summary and Discussion 56
Acknowledgments 58
References 58

"9065_c001.tex" — page 1[#1] 20/11/2008 18:51

1.1 INTRODUCTION

Many systems exist in multiple phases, depending on the values of external parameters, for example, temperature (T), pressure (P), and so on. In this context, consider a fluid (e.g., water), which can exist in three phases, viz., liquid, solid, and gas. The phase diagram of this fluid in the (T, P)-plane is shown in Figure 1.1. The chosen phase at a particular (T, P)-value is the one with lowest Gibbs potential $G(T, P)$. This phase diagram is characterized by a range of fascinating features, for example, lines of first-order phase transitions, a second-order critical point, a triple point, and so on. The correct understanding of these features is of great scientific and technological importance. We have gained a thorough understanding of the equilibrium aspects of phase transitions (and phase diagrams) through many important works, starting with the seminal contribution of Van der Waals [1,2].

There is also a fascinating class of problems involving the *kinetics of phase transitions*, that is, the evolution dynamics of a system that is rendered thermodynamically unstable by a rapid change of parameters. In the context of Figure 1.1, consider a situation in which the fluid in the solid phase is rapidly heated to a temperature where the preferred equilibrium state is the liquid phase. Clearly, the solid will convert to liquid on some timescale, so the initial and final states of the system are well understood. However, we have less knowledge about the dynamical processes that occur as the solid converts to liquid. These processes play a crucial role in our everyday life. Over the years, our understanding of the kinetics of phase transitions has improved greatly [3–6]. This book provides an overview of developments in this area.

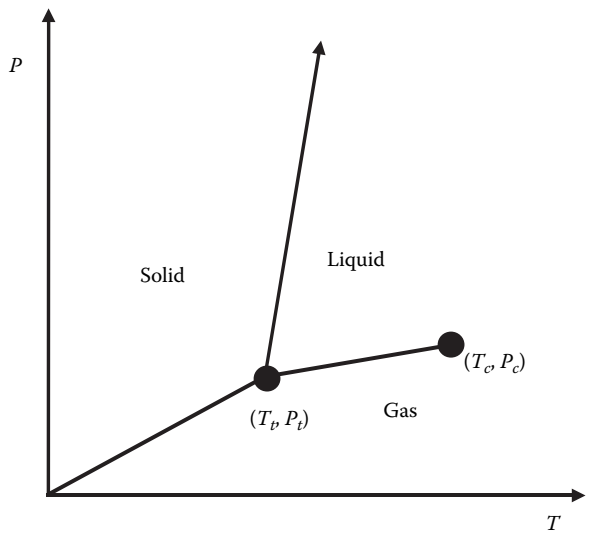

FIGURE 1.1 Phase diagram of a fluid in the (T, P)-plane. The system can exist in either of three phases—liquid, gas, or solid. The solid lines denote lines of first-order phase transitions. At the triple point (T_t, P_t), all three phases coexist. The point labeled (T_c, P_c) is the critical point of the system.

Before we proceed, it is relevant to develop the appropriate terminology first. One is often interested in the evolution of systems whose parameters have been drastically changed. Such systems are referred to as *far-from-equilibrium systems*, and their evolution is characterized by *nonlinear evolution equations* and *spatiotemporal pattern formation*. In most cases, we are unable to obtain exact solutions for the time-dependent evolution of the system. However, the presence of *domain boundaries* or *defects* in these systems provides a convenient analytical tool to understand the resultant pattern dynamics.

Let us consider two other problems in this context. These will serve as paradigms for understanding the kinetics of phase transitions. First, consider a ferromagnet whose phase diagram is shown in Figure 1.2. Focus on the case with zero magnetic field ($h = 0$). At high temperatures, the magnet is in a disordered or paramagnetic state. If the temperature is suddenly quenched to $T < T_c$, this system now prefers to be in the magnetized state with spins pointing in the "up" or "down" directions. The evolution of the system is characterized by the emergence and growth of domains enriched in either up or down spins. As time $t \to \infty$, the system approaches a spontaneously magnetized state.

Second, consider a binary (AB) mixture whose phase diagram is shown in Figure 1.3. The system is mixed or homogeneous at high temperatures. At time $t = 0$, the mixture is suddenly quenched below the *coexistence curve* or *miscibility gap*. This system now prefers to be in the phase-separated state and proceeds to its equilibrium state via the growth of domains that are either A-rich or B-rich. The nonequilibrium dynamics of the magnet or binary mixture is usually referred to as *domain growth* or *coarsening* or *phase-ordering kinetics*.

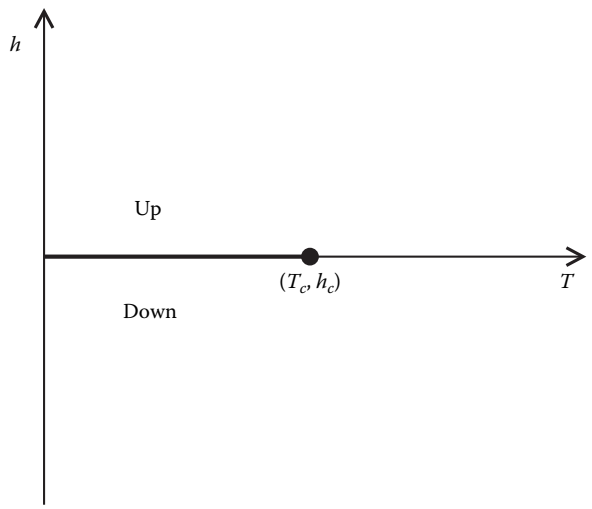

FIGURE 1.2 Phase diagram of a ferromagnet. The system parameters are the temperature (T) and the magnetic field (h). The point $(T_c, h_c = 0)$ is a second-order critical point. The line $(T < T_c, h = 0)$ corresponds to a line of first-order transitions. At low temperatures ($T < T_c$), the system can be in either of two phases, up or down, depending on the orientation of the magnetic spins.

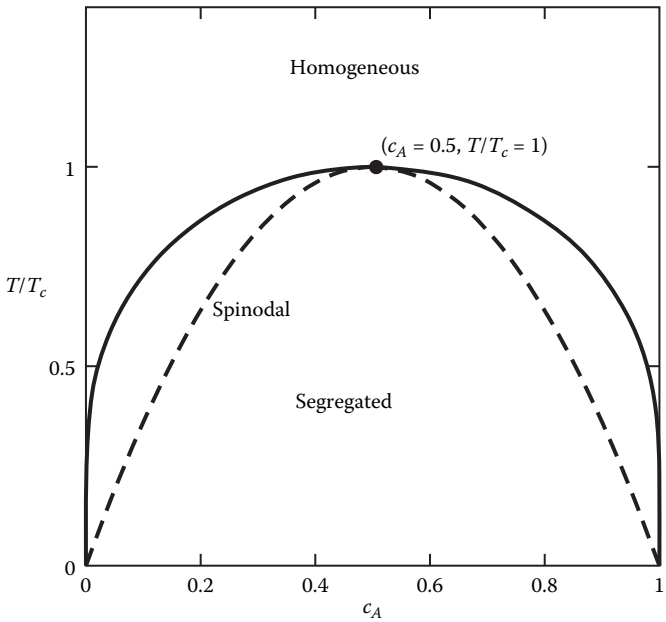

FIGURE 1.3 Phase diagram of a binary (AB) mixture. The system parameters are the concentration of A ($c_A = 1 - c_B$) and the temperature (T). The point ($c_A = 0.5, T/T_c = 1$) corresponds to a second-order critical point. Above the coexistence curve (solid line), the system is in a homogeneous or disordered state. Below the coexistence curve, the system is in a segregated or phase-separated state, characterized by A-rich and B-rich regions. The dashed lines denote spinodal curves. The homogeneous system is metastable between the coexistence and spinodal curves and unstable below the spinodal lines.

There have been many studies of the kinetics of phase transitions. Problems in this area arise in diverse contexts, ranging from *clustering dynamics in the early universe* to the *growth of nanostructures*. This book is a pedagogical exposition of developments in this area and is organized as follows. This chapter reviews the framework of phase-ordering kinetics and develops the tools and terminology used in later chapters. The subsequent chapters are written by leading experts in this area and focus on problems of special interest in the context of phase-ordering dynamics. All the chapters are written in textbook style and are accessible at the level of the advanced undergraduate student. At this point, we should stress that our understanding of this area has been greatly facilitated by numerical simulations of appropriate models. Therefore, two chapters of this book are dedicated to tutorial-level discussions of numerical simulations in this field. The first of these is written by Barkema (Chapter 3)—this chapter focuses on Monte Carlo simulations of *kinetic Ising models*. The second of these is written by Gonnella and Yeomans (Chapter 4) and describes the application of *lattice Boltzmann algorithms* to study phase-ordering systems.

This chapter is organized as follows. In Section 1.2, we introduce the Ising model for two-component mixtures and study its equilibrium properties in the mean-field (MF) approximation. This will enable us to obtain the phase diagrams shown in

Figures 1.2 and 1.3. In Section 1.3, we study kinetic versions of the Ising model. In Section 1.4, we discuss domain growth with a *nonconserved order parameter*, for example, ordering dynamics of a ferromagnet into up and down phases. In this section, we separately examine cases with scalar and vector order parameters. In Section 1.5, we discuss domain growth with a *conserved order parameter*, for example, kinetics of phase separation of an AB mixture. We will separately focus on segregation in binary alloys that is driven by diffusion, and segregation in binary fluids where flow fields drastically modify the asymptotic behavior. Finally, Section 1.6 concludes this chapter with a summary and discussion.

1.2 PHASE DIAGRAMS OF TWO-COMPONENT MIXTURES

1.2.1 Ising Model and Its Applications

The simplest model of an interacting many-body system is the Ising model [7], which was first introduced as a model for phase transitions in magnetic systems. However, with suitable generalizations, it has wide applications to diverse problems in condensed matter physics.

Consider a set of N spins $\{S_i\}$, which are fixed on the sites $\{i\}$ of a lattice. The two-state (spin-1/2) Ising Hamiltonian has the following form:

$$H = -J \sum_{\langle ij \rangle} S_i S_j, \quad S_i = \pm 1, \tag{1.1}$$

where J is the strength of the exchange interaction between spins. We consider the case with nearest-neighbor interactions only, denoted by the subscript $\langle ij \rangle$ in Equation 1.1.

Although the Hamiltonian in Equation 1.1 is formulated for a magnetic system, it is clear that a similar description applies for any interacting two-state system, as the two states can be mapped onto $S = +1$ or -1. A well-known example is the lattice gas or binary (AB) mixture [7]. We can describe this system in terms of occupation-number variables $n_i^\alpha = 1$ or 0, depending on whether or not a site i is occupied by species α(A or B). Clearly, $n_i^A + n_i^B = 1$ for all sites. A more convenient description is obtained in terms of spin variables $S_i = 2n_i^A - 1 = 1 - 2n_i^B$. We associate an interaction energy $-\epsilon_{\alpha\beta}$ between species α and β, located at neighboring sites i and j, respectively. The corresponding Hamiltonian is

$$\begin{aligned} H &= -\sum_{\langle ij \rangle} \left[\epsilon_{AA} n_i^A n_j^A + \epsilon_{BB} n_i^B n_j^B + \epsilon_{AB} \left(n_i^A n_j^B + n_i^B n_j^A \right) \right] \\ &= -\left(\frac{\epsilon_{AA} + \epsilon_{BB} - 2\epsilon_{AB}}{4} \right) \sum_{\langle ij \rangle} S_i S_j - \frac{q(\epsilon_{AA} - \epsilon_{BB})}{4} \sum_{i=1}^{N} S_i \\ &\quad - \frac{Nq}{8} (\epsilon_{AA} + \epsilon_{BB} + 2\epsilon_{AB}). \end{aligned} \tag{1.2}$$

In Equation 1.2, q denotes the coordination number of a lattice site. The second term on the right-hand side (RHS) is constant because $\sum_i S_i = N_A - N_B$, where N_α is the

number of α-atoms in the system. Further, the third term on the RHS is also a constant. The Hamiltonian in Equation 1.2 is analogous to that in Equation 1.1 if we identify

$$J = \frac{\epsilon_{AA} + \epsilon_{BB} - 2\epsilon_{AB}}{4}. \tag{1.3}$$

The Ising model and its variants are not restricted to two-state systems and can be easily generalized to the case of multiple-state systems. Thus, three-state systems can be mapped onto a spin-1 Hamiltonian; four-state systems onto a spin-3/2 Hamiltonian; and so on. In general, higher-spin models have a larger number of possible interaction terms (and parameters) in the Hamiltonian.

We can obtain phase diagrams for magnets (cf. Figure 1.2) and binary mixtures (cf. Figure 1.3) by studying the Ising model in the mean-field (MF) approximation, as described below.

1.2.2 Phase Diagrams in the Mean-Field Approximation

The equilibrium properties of the Ising model in Equation 1.1 are described in the MF approximation by the Bragg–Williams (BW) form of the Gibbs free energy [7]. This is obtained as follows. Consider a homogeneous state with spatially uniform magnetization $\langle S_i \rangle = \psi$. We approximate the energy as

$$E(\psi) \simeq -J \sum_{\langle ij \rangle} \langle S_i \rangle \langle S_j \rangle = -\frac{NqJ}{2}\psi^2. \tag{1.4}$$

The corresponding probabilities for a site to have up (↑) or down (↓) spins are

$$\begin{aligned} p_\uparrow &= \frac{1+\psi}{2}, \\ p_\downarrow &= \frac{1-\psi}{2}. \end{aligned} \tag{1.5}$$

Therefore, the entropy for a lattice with N sites is

$$S(\psi) = -Nk_B \left[\left(\frac{1+\psi}{2} \right) \ln \left(\frac{1+\psi}{2} \right) + \left(\frac{1-\psi}{2} \right) \ln \left(\frac{1-\psi}{2} \right) \right], \tag{1.6}$$

where k_B is the Boltzmann constant.

Then, the Gibbs free energy is obtained as

$$G(\psi) = E(\psi) - hM - TS(\psi), \tag{1.7}$$

where h is the magnetic field, and M $(=N\psi)$ is the overall magnetization.

This yields the free energy per spin as

$$g(T,h,\psi) = \frac{G(T,h,\psi)}{N} = -\frac{1}{2}qJ\psi^2 - h\psi + k_BT\left[\left(\frac{1+\psi}{2}\right)\ln\left(\frac{1+\psi}{2}\right) + \left(\frac{1-\psi}{2}\right)\ln\left(\frac{1-\psi}{2}\right)\right]. \tag{1.8}$$

The RHS of Equation 1.8 is a variational function of the magnetization $\psi = \langle S_i \rangle$. If we Taylor-expand the entropy term in Equation 1.8, the Gibbs free energy assumes the customary ψ^4-form:

$$g(T,h,\psi) = \frac{1}{2}\left(k_BT - qJ\right)\psi^2 - h\psi + \frac{k_BT}{12}\psi^4 + O(\psi^6) - k_BT\ln 2. \tag{1.9}$$

The order parameter ψ in Equation 1.8 or Equation 1.9 can describe both ferromagnetic and antiferromagnetic order, with $J < 0$ in the latter case. Furthermore, in the antiferromagnetic case, ψ refers to the *sublattice magnetization* or *staggered magnetization* [7].

The equilibrium value of ψ at fixed (T,h) is obtained from Equation 1.8 by minimizing the Gibbs free energy:

$$\left.\frac{\partial g}{\partial \psi}\right|_{\psi=\psi_0} = 0. \tag{1.10}$$

This yields the well-known transcendental equation [$\beta = (k_BT)^{-1}$]:

$$\psi_0 = \tanh(\beta qJ\psi_0 + \beta h). \tag{1.11}$$

For $h = 0$, we identify the MF critical temperature

$$T_c = \frac{qJ}{k_B}. \tag{1.12}$$

For $T > T_c$ and $h = 0$, the transcendental equation has only one solution $\psi_0 = 0$, which corresponds to the paramagnetic state. For $T < T_c$, Equation 1.11 has three solutions $\psi_0 = 0, \pm\psi(T)$. The state with $\psi_0 = 0$ has a higher free energy than do the equivalent states $+\psi(T)$ and $-\psi(T)$. Further, $\psi(T) \to 1$ as $T \to 0$, and $\psi(T) \to 0$ as $T \to T_c^-$. The relevant phase diagram in the (T,h)-plane is shown in Figure 1.2.

Next, let us consider the case of the binary mixture (or lattice gas) with N_A $(=c_AN)$ atoms of species A and N_B $(=c_BN)$ atoms of species B $(N = N_A + N_B)$. The appropriate order parameter in this case is the local density difference, $\psi = \langle n_i^A \rangle - \langle n_i^B \rangle$. The above analysis has to be modified because the appropriate ensemble for a binary

mixture is characterized by a fixed *magnetization* rather than a fixed *magnetic field*. The relevant free energy to be minimized is the Helmholtz potential

$$F(T,\psi) = E(\psi) - TS(\psi). \tag{1.13}$$

For the BW free energy, we have the expression

$$\begin{aligned} f(T,\psi) &= \frac{F(T,\psi)}{N} \\ &= -\frac{1}{2}qJ\psi^2 + k_BT\left[\left(\frac{1+\psi}{2}\right)\ln\left(\frac{1+\psi}{2}\right) + \left(\frac{1-\psi}{2}\right)\ln\left(\frac{1-\psi}{2}\right)\right]. \end{aligned} \tag{1.14}$$

For a system that undergoes phase separation, there are two possibilities:

(a) We can have a *homogeneous* (or one-phase) state with order parameter $\psi_h = c_A - c_B$.
(b) We can have a *phase-separated* state where the system segregates into two regions having order parameter ψ_1 (with fraction x) and ψ_2 [with fraction $(1-x)$]. The quantity x is determined from the lever rule

$$\psi_h = x\psi_1 + (1-x)\psi_2. \tag{1.15}$$

Let us minimize the Helmholtz potential $\overline{f}$ for the phase-separated state. (The homogeneous state is the limit $\psi_1 = \psi_2$.) The quantity $\overline{f}$ is obtained as

$$\overline{f} = xf(\psi_1) + (1-x)f(\psi_2). \tag{1.16}$$

This has to be minimized subject to the constraint in Equation 1.15. We implement this constraint by introducing the Lagrange multiplier λ and minimizing the quantity

$$A = xf(\psi_1) + (1-x)f(\psi_2) - \lambda[x\psi_1 + (1-x)\psi_2 - \psi_h]. \tag{1.17}$$

This yields the equations

$$\begin{aligned} \frac{\partial A}{\partial x} &= f(\psi_1) - f(\psi_2) - \lambda(\psi_1 - \psi_2) = 0, \\ \frac{\partial A}{\partial \psi_1} &= xf'(\psi_1) - \lambda x = 0, \\ \frac{\partial A}{\partial \psi_2} &= (1-x)f'(\psi_2) - \lambda(1-x) = 0, \\ \frac{\partial A}{\partial \lambda} &= x\psi_1 + (1-x)\psi_2 - \psi_h = 0. \end{aligned} \tag{1.18}$$

The first three equations yield

$$\lambda = \frac{f(\psi_1) - f(\psi_2)}{\psi_1 - \psi_2} = f'(\psi_1) = f'(\psi_2), \tag{1.19}$$

which is referred to as Maxwell's double-tangent construction. This is valid for arbitrary functional forms of the Helmholtz free energy.

The specific form for $f(T, \psi)$ in Equation 1.14 is an even function of ψ with $f(T, -\psi) = f(T, \psi)$. Further, $f(T, \psi)$ has a single minimum at $\psi = 0$ for $T > T_c = qJ$. Thus, the only solution of the double-tangent construction is $\psi_1 = \psi_2$. In that case, the constraint in Equation 1.15 yields $\psi_1 = \psi_h$, corresponding to the homogeneous state.

For $T < T_c$, $f(T, \psi)$ has a symmetric double-well structure with extrema at $f'(T, \psi_0) = 0$, that is,

$$\psi_0 = \tanh(\beta q J \psi_0). \tag{1.20}$$

The states with non-zero ψ_0 correspond to lower free energy than the state with $\psi_0 = 0$. Thus, a possible solution to the double-tangent construction is

$$\psi_1 = -\psi_0, \quad \psi_2 = +\psi_0, \tag{1.21}$$

where ψ_0 is the positive solution of Equation 1.20. However, this is only an acceptable solution if the lever rule can be satisfied, that is, $-\psi_0 < \psi_h < \psi_0$. Thus, phase separation occurs at $T < T_c$ only if $|\psi_h| < \psi_0$. When phase separation does occur, the segregated states have the composition $-\psi_0$ (B-rich) and $+\psi_0$ (A-rich), respectively. The resultant phase diagram in the $(c_A, T/T_c)$-plane is shown in Figure 1.3.

The phase diagrams in Figures 1.2 and 1.3 will provide the basis for our subsequent discussion of phase-ordering dynamics.

1.3 KINETIC ISING MODELS

1.3.1 Introduction

The above discussion has clarified the utility of Ising-like models in a wide range of problems. We next consider the issue of *kinetics of Ising models*. For simplicity, we restrict our discussion to the spin-1/2 model described by Equation 1.1. The generalization to higher-spin models is straightforward. The Ising spin variables do not have intrinsic dynamics, as is seen by constructing the relevant Poisson bracket. In order to associate kinetics with the Ising model, we assume that it is placed in contact with a heat bath that generates stochastic spin-flips ($S_i \to -S_i$) in the system [6]. The heat bath can be interpreted as consisting of phonons that induce spin-flips via a spin-lattice coupling. The resultant *kinetic Ising model* is referred to as the spin-flip or Glauber model [8] and is appropriate for describing the nonconserved kinetics of the paramagnetic $\to$ ferromagnetic transition. The probability of a jump depends on the configuration of all other spins and the heat-bath temperature, in general.

Next, consider the case where the Ising model describes a lattice gas or a binary (AB) mixture. The appropriate microscopic kinetics involves the diffusion of atoms, for example, atomic jumps to vacant sites in the lattice gas, or $A \leftrightarrow B$ interchanges in the binary mixture. Thus, the heat bath causes spin-exchanges rather than spin-flips, that is, S_i jumps from $+1 \rightarrow -1$ while a neighbor S_j *simultaneously* jumps from $-1 \rightarrow +1$. This process mimics phonon-induced atomic jumps. The resultant model is referred to as the spin-exchange or Kawasaki model [9,10].

It should be emphasized that transition probabilities in both the Glauber and Kawasaki models must satisfy the *detailed-balance condition* [11], which will be discussed shortly. Thus, although the two models describe different time-dependent behavior, the equilibrium state is *unique*. As $t \rightarrow \infty$, we recover properties calculable from the *equilibrium* statistical mechanics of the Ising model in an appropriate ensemble.

1.3.2 The Spin-Flip Glauber Model

In the Glauber model, the heat bath induces fluctuations in the system in the form of single-spin-flip processes [8]. The Glauber model describes nonconserved kinetics because the spin-flip processes make the total magnetization $M = \sum_{i=1}^{N} S_i$ time-dependent. Let us examine the evolution of the probability distribution for the spin configuration $\{S_i\}$ of a system with N spins. In this context, we introduce the conditional probability $P(\{S_i^0\}, 0|\{S_i\}, t)$, which is the probability that the ith spin is in state S_i $(i = 1 \rightarrow N)$ at time t, given that it was in state S_i^0 $(i = 1 \rightarrow N)$ at time $t = 0$. The evolution of P is described by the master equation [11]:

$$\begin{aligned}\frac{d}{dt}P(\{S_i\}, t) = &-\sum_{j=1}^{N} W(S_1, \ldots S_j, \ldots S_N|S_1, \ldots -S_j, \ldots S_N)P(\{S_i\}, t) \\ &+\sum_{j=1}^{N} W(S_1, \ldots -S_j, \ldots S_N|S_1, \ldots S_j, \ldots S_N)P(\{S_i'\}, t), \qquad (1.22)\end{aligned}$$

where we suppress the argument $(\{S_i^0\}, 0|$, for compactness. The first term on the RHS of Equation 1.22 corresponds to the *loss of probability* for the state $\{S_i\}$ due to the spin-flip $S_j \rightarrow -S_j$. The second term on the RHS denotes the *gain of probability* for the state $\{S_i\}$ due to a spin-flip $S_j' \rightarrow -S_j'$ in a state $\{S_i'\}$ with

$$\begin{aligned}S_i' &= S_i \quad \text{for } i \neq j, \\ S_j' &= -S_j. \end{aligned} \qquad (1.23)$$

Equation 1.22 assumes that the underlying stochastic process is Markovian. The essential physical input is provided by the modeling of the *transition matrix* $W(\{S_i\}|\{S_i'\})$ for the change $\{S_i\}$ to $\{S_i'\}$). The choice of W must be such that the

ensemble approaches the equilibrium distribution $P_{\text{eq}}(\{S_i\})$ as $t \to \infty$:

$$P_{\text{eq}}(\{S_i\}) = \frac{1}{Z(T,h,N)} \exp[-\beta(H - hM)]. \tag{1.24}$$

Here, Z is the partition function, which is defined as

$$Z(T,h,N) = \sum_{\{S_i\}} \exp[-\beta(H - hM)]. \tag{1.25}$$

To ensure this, the transition probability $W(\{S_i\}|\{S_i'\})$ should obey the *detailed-balance condition* [11]:

$$W\big(\{S_i\}|\{S_i'\}\big)P_{\text{eq}}(\{S_i\}) = W\big(\{S_i'\}|\{S_i\}\big)P_{\text{eq}}\big(\{S_i'\}\big). \tag{1.26}$$

Clearly, in the equilibrium ensemble, this guarantees that the number of systems making the transition from $\{S_i\} \to \{S_i'\}$ is balanced by the number of systems making the reverse transition $\{S_i'\} \to \{S_i\}$. Thus, the probability distribution P_{eq} is independent of time, as expected. Further, an arbitrary distribution $P(\{S_i\}, t) \to P_{\text{eq}}(\{S_i\})$ as $t \to \infty$ under Equation 1.22, provided that W obeys the detailed-balance condition. For the proof of this, we refer the reader to the book by Van Kampen [11].

It is evident that there are many choices of W that satisfy the condition in Equation 1.26. We choose the Suzuki–Kubo form [12]:

$$W\big(\{S_i\}|\{S_i'\}\big) = \frac{\lambda}{2}\left\{1 - \tanh\left[\frac{\beta\Delta(H - hM)}{2}\right]\right\}, \tag{1.27}$$

where λ^{-1} sets the timescale of the nonequilibrium process. Here, $\Delta(H - hM)$ denotes the enthalpy difference between the final state $\{S_i'\}$ and the initial state $\{S_i\}$. It is straightforward to confirm that this form of W satisfies the detailed-balance condition.

For the spin-flip Ising model, the states $\{S_i'\}$ and $\{S_i\}$ differ only in one spin, that is, $S_j' = -S_j$. Then

$$\begin{aligned}(H - hM)_{\text{initial}} &= -JS_j \sum_{L_j} S_{L_j} - hS_j + \text{other terms},\\ (H - hM)_{\text{final}} &= JS_j \sum_{L_j} S_{L_j} + hS_j + \text{other terms},\end{aligned} \tag{1.28}$$

where L_j denotes the nearest neighbors (nn) of j. Thus

$$\Delta(H - hM) = 2JS_j \sum_{L_j} S_{L_j} + 2hS_j, \tag{1.29}$$

and

$$W\left(\{S_i\}|\{S_i'\}\right) = \frac{\lambda}{2}\left[1 - \tanh\left(\beta J S_j \sum_{L_j} S_{L_j} + \beta h S_j\right)\right]$$
$$= \frac{\lambda}{2}\left[1 - S_j \tanh\left(\beta J \sum_{L_j} S_{L_j} + \beta h\right)\right]. \tag{1.30}$$

In Equation 1.30, we can bring S_j outside the argument of the tanh-function because it only takes the values $+1$ or -1. We replace the form of W from Equation 1.30 in Equation 1.22 to obtain the explicit form of the master equation:

$$\frac{d}{dt}P(\{S_i\},t) = -\frac{\lambda}{2}\sum_{j=1}^{N}\left[1 - S_j \tanh\left(\beta J \sum_{L_j} S_{L_j} + \beta h\right)\right]P(\{S_i\},t)$$
$$+ \frac{\lambda}{2}\sum_{j=1}^{N}\left[1 + S_j \tanh\left(\beta J \sum_{L_j} S_{L_j} + \beta h\right)\right]P\left(\{S_i'\},t\right). \tag{1.31}$$

We can use this master equation to obtain the evolution of the magnetization:

$$\langle S_k\rangle = \sum_{\{S_i\}} S_k P(\{S_i\},t). \tag{1.32}$$

We multiply both sides of Equation 1.31 by S_k and sum over all configurations to obtain

$$\frac{d}{dt}\langle S_k\rangle = -\frac{\lambda}{2}\sum_{j=1}^{N}\sum_{\{S_i\}} S_k\left[1 - S_j \tanh\left(\beta J \sum_{L_j} S_{L_j} + \beta h\right)\right]P(\{S_i\},t)$$
$$+ \frac{\lambda}{2}\sum_{j=1}^{N}\sum_{\{S_i\}} S_k\left[1 + S_j \tanh\left(\beta J \sum_{L_j} S_{L_j} + \beta h\right)\right]P\left(\{S_i'\},t\right)$$
$$\equiv A + B. \tag{1.33}$$

In the second term on the RHS of Equation 1.33, we redefine $S_j = -\overline{S_j}$. Clearly, the sum $\sum_{S_j=\pm1}$ is equivalent to the sum $\sum_{\overline{S_j}=\pm1}$. Therefore, the terms in A and B cancel

with each other, except for the case $j = k$. This yields the following evolution equation for the magnetization:

$$\lambda^{-1}\frac{d}{dt}\langle S_k\rangle = -\sum_{\{S_i\}} S_k\left[1 - S_k \tanh\left(\beta J\sum_{L_k} S_{L_k} + \beta h\right)\right] P(\{S_i\}, t)$$
$$= -\langle S_k\rangle + \left\langle \tanh\left(\beta J\sum_{L_k} S_{L_k} + \beta h\right)\right\rangle, \tag{1.34}$$

where we have used $S_k^2 = 1$.

1.3.2.1 Mean-Field Approximation

Unfortunately, the exact time-dependent Equation 1.34 is analytically intractable in $d \geq 2$. (For the $d = 1$ solution, see the work of Glauber [8].) The main obstacle is that the second term on the RHS of Equation 1.34 yields a set of higher-order correlation functions, as can be seen by expanding the tanh-function. These dynamical equations can be rendered tractable by invoking the MF approximation, which truncates the hierarchy by neglecting correlations between different sites, that is, the average of the product of spin operators is replaced by the product of their averages. The result of such a random-phase decoupling is that the angular brackets denoting the statistical average can be taken inside the argument of the tanh-function [13,14]. Thus, we obtain

$$\lambda^{-1}\frac{d}{dt}\langle S_k\rangle = -\langle S_k\rangle + \tanh\left(\beta J\sum_{L_k}\langle S_{L_k}\rangle + \beta h\right). \tag{1.35}$$

For time-independent effects in equilibrium, the LHS of Equation 1.35 is identically zero. Thus, we have (as $t \to \infty$)

$$\langle S_k\rangle^{\mathrm{eq}} = \tanh\left(\beta J\sum_{L_k}\langle S_{L_k}\rangle^{\mathrm{eq}} + \beta h\right). \tag{1.36}$$

Notice that Equation 1.35 is nonlinear because of the presence of the tanh-function and is only tractable numerically. These equations are often referred to as *mean-field dynamical models* in the literature [15–19]. A further simplification can be effected by expanding the tanh-function and retaining only leading terms. For simplicity, we consider the case of zero magnetic field, that is, $h = 0$. We can then expand various

terms on the RHS of Equation 1.35 as follows:

$$\sum_{L_k} \langle S_{L_k} \rangle \simeq q\psi(\vec{r}_k, t) + a^2 \nabla_k^2 \psi(\vec{r}_k, t) + \text{higher-order terms}, \tag{1.37}$$

where a is the lattice spacing. Further,

$$\begin{aligned} \tanh\left(\beta J \sum_{L_k} \langle S_{L_k} \rangle\right) &\simeq \beta J \sum_{L_k} \langle S_{L_k} \rangle - \frac{1}{3}\left(\beta J \sum_{L_k} \langle S_{L_k} \rangle\right)^3 + \text{ higher-order terms} \\ &\simeq \frac{T_c}{T}\psi(\vec{r}_k, t) - \frac{1}{3}\left(\frac{T_c}{T}\right)^3 \psi(\vec{r}_k, t)^3 + \frac{T_c}{qT} a^2 \nabla_k^2 \psi\,(\vec{r}_k, t) \\ &\quad + \text{other terms}, \end{aligned} \tag{1.38}$$

where we have used Equation 1.37 to obtain the second expression. Therefore, the order-parameter equation for the Glauber–Ising model simplifies as

$$\lambda^{-1} \frac{\partial}{\partial t}\psi(\vec{r}, t) = \left(\frac{T_c}{T} - 1\right)\psi - \frac{1}{3}\left(\frac{T_c}{T}\right)^3 \psi^3 + \frac{T_c}{qT} a^2 \nabla^2 \psi + \text{other terms}, \tag{1.39}$$

where we have dropped the subscript k for the position variable.

At this stage, a few remarks are in order. Firstly, Equation 1.39 is referred to as the *time-dependent Ginzburg–Landau* (TDGL) equation. We will discuss the general formulation of the TDGL equation in Section 1.4.1. Secondly, the approximation of neglecting the higher-order terms in Equation 1.39 is justifiable only for $T \simeq T_c$, where the order parameter is small. However, it is generally believed that the TDGL equation is valid even for deep quenches ($T \ll T_c$), at least in terms of containing the correct physics.

1.3.3 The Spin-Exchange Kawasaki Model

We mentioned earlier that the Glauber model, which assumes single-spin-flip processes, is appropriate for nonconserved kinetics. On the other hand, when the Ising model describes either phase separation ($J > 0$) or order-disorder ($J < 0$) transitions in an AB mixture [1,7,20,21], the Glauber model is not applicable. For a binary mixture, the Ising spin variable models the presence of an A- or B-atom on a lattice site. Thus, the appropriate microscopic dynamics should involve random exchanges of A- and B-atoms at neighboring sites, with their individual numbers being constant. In practice, these jumps are actually mediated by vacancies [22–25], and the system should be described as a ternary (ABV) mixture [18,19,26,27]. However, when the vacancy concentration is small, it is reasonable to ignore vacancies and assume that the underlying stochastic process is a spin-exchange. As stated

earlier, this corresponds to the Kawasaki model, which is based on a stationary Markov process involving a spin-exchange mechanism [9,10]. The resultant master equation is as follows:

$$\frac{d}{dt}P(\{S_i\},t) = -\sum_{j=1}^{N}\sum_{k\in L_j} W(S_1,\ldots S_j,S_k,\ldots S_N|S_1,\ldots S_k,S_j,\ldots S_N)P(\{S_i\},t) + \sum_{j=1}^{N}\sum_{k\in L_j} W(S_1,\ldots S_k,S_j,\ldots S_N|S_1,\ldots S_j,S_k,\ldots S_N)P(\{S_i'\},t). \tag{1.40}$$

The first term on the RHS is the loss of probability for the state $\{S_i\}$ due to the spin-exchange $S_j \leftrightarrow S_k$. We consider only nearest-neighbor exchanges, where site $k \in L_j$, that is, the nearest-neighbors of j. The second term on the RHS corresponds to the gain of probability for the state $\{S_i\}$ due to an exchange $S_j' \leftrightarrow S_k'$ in a state $\{S_i'\}$. The state $\{S_i'\}$ differs from the state $\{S_i\}$ in only two spins:

$$\begin{aligned} S_i' &= S_i \quad \text{for} \quad i \neq j,k, \\ S_j' &= S_k, \\ S_k' &= S_j. \end{aligned} \tag{1.41}$$

As in the Glauber case, the transition probability $W(\{S_i\}|\{S_i'\})$ must obey the detailed-balance condition. As we have seen in Section 1.2.2, the binary mixture is described by an ensemble with fixed (T,M,N), where the "magnetization" $M = \sum_{i=1}^{N} S_i = N_A - N_B$. The corresponding equilibrium distribution is

$$P_{\text{eq}}(\{S_i\}) = \frac{1}{Z(T,M,N)}\exp(-\beta H)\delta_{\sum_i S_i,M}, \tag{1.42}$$

where the Kronecker delta confines the distribution to configurations with $\sum_{i=1}^{N} S_i = M$. The appropriate partition function is

$$Z(T,M,N) = \sum_{\{S_i\}} \exp(-\beta H)\delta_{\sum_i S_i,M}. \tag{1.43}$$

Again, we choose the Suzuki–Kubo form for the transition probability in Equation 1.40:

$$W(\{S_i\}|\{S_i'\}) = \frac{\lambda}{2}\left[1 - \tanh\left(\frac{\beta\Delta H}{2}\right)\right], \tag{1.44}$$

where ΔH is the change in energy due to the spin-exchange $S_j \leftrightarrow S_k$. For the Ising model,

$$\begin{aligned} H_{\text{initial}} &= -JS_j \sum_{L_j \neq k} S_{L_j} - JS_k \sum_{L_k \neq j} S_{L_k} - JS_jS_k + \text{other terms}, \\ H_{\text{final}} &= -JS_k \sum_{L_j \neq k} S_{L_j} - JS_j \sum_{L_k \neq j} S_{L_k} - JS_jS_k + \text{other terms}. \end{aligned} \tag{1.45}$$

Thus, the energy change resulting from the spin exchange is

$$\Delta H = J(S_j - S_k) \sum_{L_j \neq k} S_{L_j} - J(S_j - S_k) \sum_{L_k \neq j} S_{L_k}, \tag{1.46}$$

and

$$\begin{aligned} W\big(\{S_i\}|\{S_i'\}\big) &= \frac{\lambda}{2}\left\{1 - \tanh\left[\frac{\beta J}{2}(S_j - S_k)\sum_{L_j \neq k} S_{L_j} - \frac{\beta J}{2}(S_j - S_k)\sum_{L_k \neq j} S_{L_k}\right]\right\} \\ &= \frac{\lambda}{2}\left\{1 - \frac{S_j - S_k}{2}\tanh\left[\beta J\left(\sum_{L_j \neq k} S_{L_j} - \sum_{L_k \neq j} S_{L_k}\right)\right]\right\}. \end{aligned} \tag{1.47}$$

In Equation 1.47, we have used the fact that $(S_j - S_k)/2 = 0, \pm 1$ to factor it out of the argument of the tanh-function. Therefore, the master equation has the form

$$\begin{aligned} \frac{d}{dt}P(\{S_i\}, t) = &-\frac{\lambda}{2}\sum_{j=1}^{N}\sum_{k \in L_j}\left\{1 - \frac{S_j - S_k}{2}\tanh\left[\beta J\left(\sum_{L_j \neq k} S_{L_j} - \sum_{L_k \neq j} S_{L_k}\right)\right]\right\} P(\{S_i\}, t) \\ &+ \frac{\lambda}{2}\sum_{j=1}^{N}\sum_{k \in L_j}\left\{1 + \frac{S_j - S_k}{2}\tanh\left[\beta J\left(\sum_{L_j \neq k} S_{L_j} - \sum_{L_k \neq j} S_{L_k}\right)\right]\right\} P\big(\{S_i'\}, t\big). \end{aligned} \tag{1.48}$$

We can obtain an evolution equation for the order parameter by multiplying both sides of Equation 1.48 with S_n and summing over all configurations:

$$\frac{d}{dt}\langle S_n\rangle = -\frac{\lambda}{2}\sum_{\{S_i\}}\sum_{j=1}^{N}\sum_{k\in L_j} S_n\left\{1-\frac{S_j-S_k}{2}\tanh\left[\beta J\left(\sum_{L_j\neq k}S_{L_j}-\sum_{L_k\neq j}S_{L_k}\right)\right]\right\}P(\{S_i\},t)$$
$$+\frac{\lambda}{2}\sum_{\{S_i\}}\sum_{j=1}^{N}\sum_{k\in L_j} S_n\left\{1+\frac{S_j-S_k}{2}\tanh\left[\beta J\left(\sum_{L_j\neq k}S_{L_j}-\sum_{L_k\neq j}S_{L_k}\right)\right]\right\}P(\{S_i'\},t). \tag{1.49}$$

In the second term on the RHS of Equation 1.49, we redesignate $S_j = \overline{S}_k$ and $S_k = \overline{S}_j$. This leads to a large-scale cancellation between the first and second terms. The only remaining terms are

$$\frac{d}{dt}\langle S_n\rangle = -\frac{\lambda}{2}\sum_{\{S_i\}}\sum_{k\in L_n} S_n\left\{1-\frac{S_n-S_k}{2}\tanh\left[\beta J\left(\sum_{L_n\neq k}S_{L_n}-\sum_{L_k\neq n}S_{L_k}\right)\right]\right\}P(\{S_i\},t)$$
$$+\frac{\lambda}{2}\sum_{\{S_i\}}\sum_{k\in L_n} S_k\left\{1+\frac{S_k-S_n}{2}\tanh\left[\beta J\left(\sum_{L_n\neq k}S_{L_n}-\sum_{L_k\neq n}S_{L_k}\right)\right]\right\}P(\{S_i\},t)$$
$$=-\frac{\lambda}{2}\left\langle\sum_{k\in L_n}(S_n-S_k)\left\{1-\frac{S_n-S_k}{2}\tanh\left[\beta J\left(\sum_{L_n\neq k}S_{L_n}-\sum_{L_k\neq n}S_{L_k}\right)\right]\right\}\right\rangle. \tag{1.50}$$

Some algebra yields the exact evolution equation

$$2\lambda^{-1}\frac{d}{dt}\langle S_n\rangle = -q\langle S_n\rangle + \sum_{L_n}\langle S_{L_n}\rangle$$
$$+\sum_{k\in L_n}\left\langle(1-S_nS_k)\tanh\left[\beta J\left(\sum_{L_n\neq k}S_{L_n}-\sum_{L_k\neq n}S_{L_k}\right)\right]\right\rangle. \tag{1.51}$$

This equation is analogous to Equation 1.34, obtained in the context of Glauber kinetics.

Although the Kawasaki model is usually associated with conserved kinetics, we should make a clarifying remark. In the context of binary mixtures, a *ferromagnetic*

interaction ($J > 0$) results in phase separation, that is, the equilibrium system consists of domains of A-rich and B-rich phases. The appropriate order parameter is the difference in densities of A and B and is locally conserved by Kawasaki kinetics. The length scale over which the order parameter is conserved increases if we allow *long-ranged* exchanges rather than only *nearest-neighbor* exchanges. In the limit where the spin exchanges are *infinite-ranged*, the Kawasaki model has *global conservation* rather than *local conservation*. In this case, the Kawasaki model is essentially equivalent to the Glauber model [28,29].

It is also of great interest to consider the binary mixture with *antiferromagnetic* interactions, $J < 0$. In this case, there is a phase transition from a high-temperature disordered phase to a low-temperature ordered phase, where the A- and B-atoms order on alternate sub lattices. The appropriate order parameter is now the *staggered magnetization*, which is the difference between the two sub lattice *magnetizations*. This quantity is not conserved by Kawasaki kinetics, though the overall concentration is conserved. For the AB alloy with equal fractions of A and B, the antiferromagnetic case with Kawasaki kinetics is equivalent to the ferromagnetic Ising model with Glauber kinetics [30]. For asymmetric compositions, novel features arise due to the conserved concentration variable.

1.3.3.1 Mean-Field Approximation

As in the Glauber case, Equation 1.51 is the first of a hierarchy of equations involving higher-order correlations of the spin variable. This hierarchy can be truncated by invoking the MF approximation, that is, by replacing the expectation value of a function of spin variables by the function of the expectation values of the spin variables. The resultant MF dynamical model is

$$2\lambda^{-1}\frac{d}{dt}\langle S_n\rangle = -q\langle S_n\rangle + \sum_{L_n}\langle S_{L_n}\rangle + \sum_{k\in L_n}(1-\langle S_n\rangle\langle S_k\rangle)\tanh\left[\beta J\left(\sum_{L_n}\langle S_{L_n}\rangle - \sum_{L_k}\langle S_{L_k}\rangle\right)\right]. \tag{1.52}$$

Notice that the restrictions on the summations inside the tanh-function have been dropped in the MF approximation. This is necessary for Equation 1.52 to contain the correct MF solution in Equation 1.36 [13]. Recall the MF solution for the $h = 0$ case:

$$\langle S_k\rangle^{\mathrm{eq}} = \tanh\left(\beta J\sum_{L_k}\langle S_{L_k}\rangle^{\mathrm{eq}}\right). \tag{1.53}$$

If we replace this in the RHS of Equation 1.52, we obtain

$$\begin{aligned}\text{RHS} &= -q\langle S_n\rangle^{\text{eq}} + \sum_{L_n}\langle S_{L_n}\rangle^{\text{eq}} + \sum_{k\in L_n}\left(1 - \langle S_n\rangle^{\text{eq}}\,\langle S_k\rangle^{\text{eq}}\right) \\ &\quad\times\left[\frac{\tanh\left(\beta J\sum_{L_n}\left\langle S_{L_n}\right\rangle^{\text{eq}}\right) - \tanh\left(\beta J\sum_{L_k}\left\langle S_{L_k}\right\rangle^{\text{eq}}\right)}{1 - \tanh\left(\beta J\sum_{L_n}\left\langle S_{L_n}\right\rangle^{\text{eq}}\right)\tanh\left(\beta J\sum_{L_k}\left\langle S_{L_k}\right\rangle^{\text{eq}}\right)}\right] \\ &= -q\,\langle S_n\rangle^{\text{eq}} + \sum_{L_n}\left\langle S_{L_n}\right\rangle^{\text{eq}} + \sum_{L_n}\left(\langle S_n\rangle^{\text{eq}} - \left\langle S_{L_n}\right\rangle^{\text{eq}}\right) \\ &= 0, \end{aligned} \tag{1.54}$$

as expected.

Finally, let us derive a partial differential equation for the order parameter. This is the conserved counterpart of the TDGL equation we derived for the magnetization in Section 1.3.2. We can simplify the RHS of Equation 1.52 by using the identity

$$\begin{aligned}\tanh(X - Y) &= \frac{\tanh X - \tanh Y}{1 - \tanh X\tanh Y}, \quad \text{where} \\ X &= \beta J\sum_{L_n}\langle S_{L_n}\rangle, \\ Y &= \beta J\sum_{L_k}\langle S_{L_k}\rangle. \end{aligned} \tag{1.55}$$

We are interested in the late-stage dynamics, where the system has equilibrated locally and Equation 1.53 applies. Then, we make the approximation:

$$(1 - \langle S_n\rangle\langle S_k\rangle)\left(\frac{\tanh X - \tanh Y}{1 - \tanh X\tanh Y}\right) \simeq \tanh X - \tanh Y. \tag{1.56}$$

Therefore, we can rewrite Equation 1.52 as

$$\begin{aligned}2\lambda^{-1}\frac{d}{dt}\langle S_n\rangle &\simeq \sum_{L_n}\left(\langle S_{L_n}\rangle - \langle S_n\rangle\right) \\ &\quad + \sum_{k\in L_n}\left[\tanh\left(\beta J\sum_{L_n}\langle S_{L_n}\rangle\right) - \tanh\left(\beta J\sum_{L_k}\langle S_{L_k}\rangle\right)\right] \\ &= \Delta_D\left[\langle S_n\rangle - \tanh\left(\beta J\sum_{L_n}\langle S_{L_n}\rangle\right)\right], \end{aligned} \tag{1.57}$$

where Δ_D denotes the discrete Laplacian operator. We can use the Taylor expansion in Equation 1.38 to obtain the coarse-grained version of Equation 1.57 as

$$2\lambda^{-1}\frac{\partial}{\partial t}\psi(\vec{r},t) = -a^2\nabla^2\left[\left(\frac{T_c}{T}-1\right)\psi - \frac{1}{3}\left(\frac{T_c}{T}\right)^3\psi^3 + \frac{T_c}{qT}a^2\nabla^2\psi\right] + \text{other terms}, \tag{1.58}$$

where a is the lattice spacing.

Equation 1.58 is known as the Cahn–Hilliard (CH) equation and is the standard model for phase separation driven by diffusion. In Section 1.5.1, we will derive the CH equation using phenomenological arguments.

1.4 DOMAIN GROWTH IN SYSTEMS WITH NONCONSERVED KINETICS

1.4.1 Case with Scalar Order Parameter

In Figure 1.2, we had shown the phase diagram for a ferromagnet. The corresponding ordering problem considers a paramagnetic system at $T > T_c, h = 0$ for time $t < 0$. At $t = 0$, the system is rapidly quenched to $T < T_c$, where the preferred equilibrium state is spontaneously magnetized. The *far-from-equilibrium* disordered system evolves toward its new equilibrium state by separating into domains that are rich in either up or down spins (see Figure 1.4). These domains coarsen with time and are characterized by a growing length scale $L(t)$. A finite system becomes ordered in either of the two equivalent states (up or down) as $t \to \infty$.

At the microscopic level, this evolution can be described by an Ising model with Glauber spin-flip kinetics, as discussed in Section 1.3.2. At the coarse-grained level, the appropriate order parameter to describe the system is the local magnetization $\psi(\vec{r},t)$. In Section 1.3.2, we had used the Glauber–Ising model to derive the TDGL equation 1.39, which governs the evolution of the order parameter. More generally, the TDGL equation models the dissipative (over-damped) relaxation of a ferromagnetic system to its free-energy minimum:

$$\frac{\partial}{\partial t}\psi(\vec{r},t) = -\Gamma\frac{\delta G[\psi]}{\delta\psi} + \theta(\vec{r},t). \tag{1.59}$$

In Equation 1.59, Γ denotes the inverse damping coefficient; and $\delta G/\delta\psi$ is the functional derivative of the free-energy functional:

$$G[\psi] = \int d\vec{r}\left[g(\psi) + \frac{1}{2}K(\vec{\nabla}\psi)^2\right]. \tag{1.60}$$

Typical forms of the local free energy $g(\psi)$ are given in Equations 1.8 and 1.9. The second term on the RHS of Equation 1.60 accounts for surface tension due to inhomogeneities in the order parameter. The parameter K (>0) measures the strength of the surface tension.

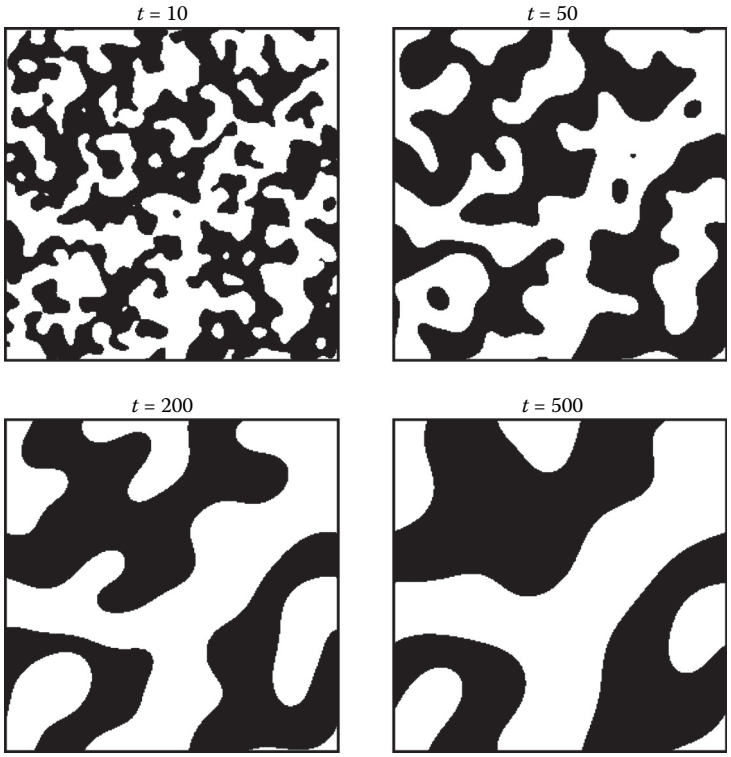

FIGURE 1.4 Evolution of a disordered ferromagnet, which is quenched to $T < T_c$ at time $t = 0$. These pictures were obtained from a Euler-discretized version of the dimensionless TDGL equation 1.66 with $h = 0$ and no thermal fluctuations ($\epsilon = 0$). The discretization mesh sizes were $\Delta t = 0.1$ and $\Delta x = 1$ in time and space, respectively. The initial condition $\psi(\vec{r}, 0)$ consisted of small-amplitude fluctuations about $\psi = 0$. The lattice size was 256^2, and periodic boundary conditions were applied in both directions. Regions with up spins ($\psi > 0$) and down spins ($\psi < 0$) are marked black and white, respectively.

The noise term in Equation 1.59 is also space- and time-dependent and satisfies the fluctuation-dissipation relation:

$$\overline{\theta(\vec{r}, t)} = 0,$$
$$\overline{\theta(\vec{r}', t')\theta(\vec{r}'', t'')} = 2\Gamma k_B T \delta(\vec{r}' - \vec{r}'')\delta(t' - t''), \tag{1.61}$$

where the bars denote an average over the Gaussian noise ensemble. The presence of the noise term ensures that the system equilibrates to the correct Boltzmann distribution at temperature T. Equations 1.59 through 1.61 are also referred to as *Model A* of order-parameter kinetics, as discussed by Hohenberg and Halperin [31] in the context of dynamic critical phenomena.

Recall the TDGL equation 1.39, which was derived in Section 1.3.2. We identify it as the deterministic version of the general form in Equation 1.59. Further, the damping coefficient $\Gamma = \beta\lambda$, where λ is the inverse timescale of Glauber spin-flips. Finally, the form of the free-energy functional that gives rise to Equation 1.39 is

$$\beta G[\psi] = \int d\vec{r} \left[-\frac{1}{2}\left(\frac{T_c}{T} - 1\right)\psi^2 + \frac{1}{12}\left(\frac{T_c}{T}\right)^3 \psi^4 + \frac{T_c}{2qT} a^2 \left(\vec{\nabla}\psi\right)^2 \right]. \quad (1.62)$$

For our subsequent discussion, it is convenient to use the general form of the ψ^4-free energy:

$$G[\psi] = \int d\vec{r} \left[-\frac{a(T_c - T)}{2}\psi^2 + \frac{b}{4}\psi^4 - h\psi + \frac{K}{2}\left(\vec{\nabla}\psi\right)^2 \right], \quad (1.63)$$

where we have introduced the parameters $a, b > 0$ and a term proportional to the magnetic field; and neglected terms of $O(\psi^6)$ and higher. The parameters a, b can be identified by a comparison with the explicit form of the free energy in (say) Equation 1.62. However, it is more appropriate to think of them as phenomenological parameters, without any reference to an underlying microscopic model.

For the ψ^4-free energy in Equation 1.63, the TDGL equation 1.59 has the form:

$$\frac{\partial}{\partial t}\psi(\vec{r}, t) = \Gamma \left[a(T_c - T)\psi - b\psi^3 + h + K\nabla^2\psi \right] + \theta(\vec{r}, t). \quad (1.64)$$

The parameters in Equation 1.64 can be absorbed into the definitions of space and time by introducing the rescaled variables (for $T < T_c$)

$$\begin{aligned}
\psi' &= \frac{\psi}{\psi_0}, \quad \psi_0 = \sqrt{\frac{a(T_c - T)}{b}}, \\
t' &= a(T_c - T)\Gamma\, t, \\
\vec{r}' &= \sqrt{\frac{a(T_c - T)}{K}}\,\vec{r}, \quad \xi_b = \sqrt{\frac{2K}{a(T_c - T)}}, \\
h' &= \frac{h}{a(T_c - T)\psi_0}, \\
\theta' &= \frac{\theta}{a(T_c - T)\Gamma\psi_0}.
\end{aligned} \quad (1.65)$$

Dropping primes, we obtain the dimensionless TDGL equation:

$$\frac{\partial}{\partial t}\psi(\vec{r}, t) = \psi - \psi^3 + h + \nabla^2\psi + \theta(\vec{r}, t), \quad (1.66)$$

where

$$\overline{\theta(\vec{r},t)} = 0,$$
$$\overline{\theta(\vec{r}',t')\theta(\vec{r}'',t'')} = 2\epsilon\delta(\vec{r}'-\vec{r}'')\delta(t'-t''),$$
$$\epsilon = \frac{k_B T b\,[a(T_c - T)]^{(d-4)/2}}{K^{d/2}}. \tag{1.67}$$

We will focus on the case with $h = 0$ (shown in Figure 1.4), where the system evolves into two competing states. There is a *domain boundary* or *interface* that separates regions enriched in the two states. Our analytical understanding of domain growth problems is based on the dynamics of these interfaces.

1.4.1.1 Static Interfaces or Kinks

Consider the deterministic version of the TDGL equation with $h = 0$:

$$\frac{\partial}{\partial t}\psi(\vec{r},t) = \psi - \psi^3 + \nabla^2\psi, \tag{1.68}$$

where we have set $\epsilon = 0$ in Equation 1.66. The static solution of this equation corresponds to a uniform state with $\psi_0 = +1$ or $\psi_0 = -1$. Another static solution (with higher energy than that of the uniform state) is the *interface* or *kink*, which is obtained as the solution of

$$\frac{d^2\psi_s}{dz^2} + \psi_s - \psi_s^3 = 0. \tag{1.69}$$

The kink solution is

$$\psi_s(z) = \tanh\left[\pm\frac{(z - z_0)}{\sqrt{2}}\right], \tag{1.70}$$

where z_0 (the center of the kink) is arbitrary. The solutions with a positive sign (kink) and negative sign (anti-kink) are shown in Figure 1.5. The kink (anti-kink) goes from $\psi = -1$ ($\psi = +1$) at $z = -\infty$ to $\psi = +1$ ($\psi = -1$) at $z = \infty$. The solution differs from $\psi \simeq \pm 1$ in a small interfacial region only, whose width defines the correlation length $\xi_b = \sqrt{2}$ (in dimensionless units).

The free energy associated with a configuration $\psi(\vec{r})$ is (in dimensionless units)

$$G[\psi] = \int d\vec{r}\left[-\frac{\psi^2}{2} + \frac{\psi^4}{4} + \frac{1}{2}(\vec{\nabla}\psi)^2\right]. \tag{1.71}$$

Therefore, the free-energy difference between the kink solution and the homogeneous solution $\psi = \psi_0$ is

$$\Delta G = A\int_{-\infty}^{\infty} dz\left[-\frac{1}{2}\left(\psi_s^2 - \psi_0^2\right) + \frac{1}{4}\left(\psi_s^4 - \psi_0^4\right) + \frac{1}{2}\left(\frac{d\psi_s}{dz}\right)^2\right], \tag{1.72}$$

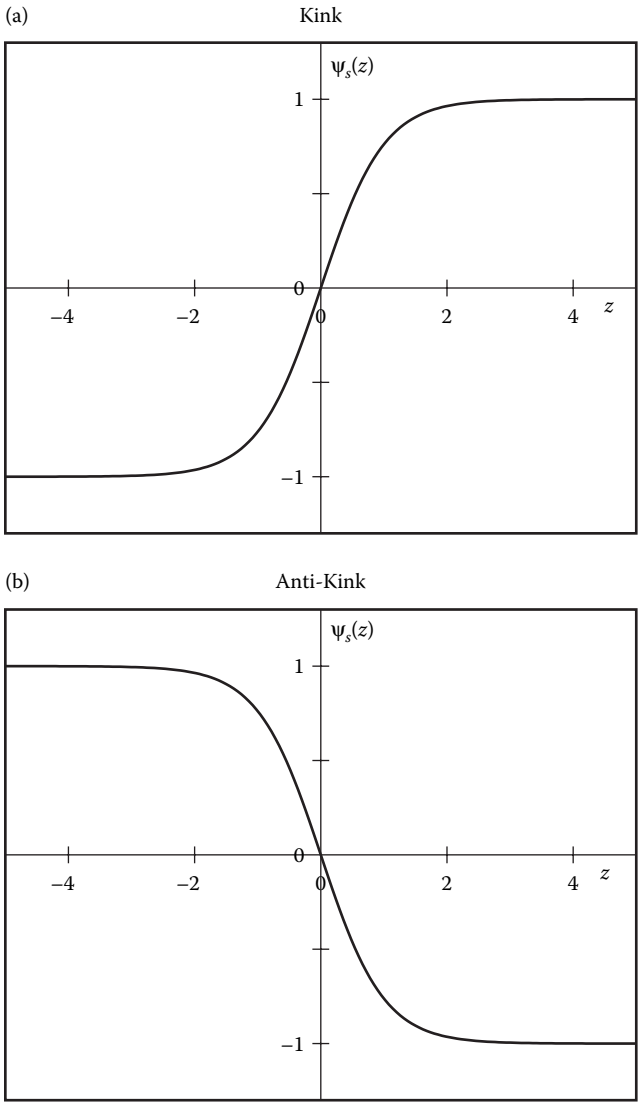

FIGURE 1.5 Variation of the order parameter [$\psi_s(z)$ versus z] for the (a) static kink profile and (b) static anti-kink profile.

where A is the area in the directions perpendicular to the z-axis. This integral is evaluated as follows. Multiply both sides of Equation 1.69 by $d\psi_s/dz$ to obtain

$$\frac{d}{dz}\left[\frac{\psi_s^2}{2} - \frac{\psi_s^4}{4} + \frac{1}{2}\left(\frac{d\psi_s}{dz}\right)^2\right] = 0. \tag{1.73}$$

We integrate this equation to obtain

$$\frac{\psi_s^2}{2} - \frac{\psi_s^4}{4} + \frac{1}{2}\left(\frac{d\psi_s}{dz}\right)^2 = C \text{ (constant)}$$
$$= \frac{\psi_0^2}{2} - \frac{\psi_0^4}{4}, \tag{1.74}$$

where we have used

$$\lim_{z\to\infty} \psi_s = \pm\psi_0,$$
$$\lim_{z\to\infty} \frac{d\psi_s}{dz} = 0. \tag{1.75}$$

Replacing Equation 1.74 in Equation 1.72, we obtain the surface tension σ as

$$\sigma = \frac{\Delta G}{A} = \int_{-\infty}^{\infty} dz \left(\frac{d\psi_s}{dz}\right)^2$$
$$= \frac{1}{2}\int_{-\infty}^{\infty} dz \,\mathrm{sech}^4\left(\frac{z}{\sqrt{2}}\right)$$
$$= \frac{2\sqrt{2}}{3}. \tag{1.76}$$

The above discussion applies to a flat interface. Clearly, the interfaces in Figure 1.4 are not flat. However, in the late stages of evolution, we expect the local order parameter to have equilibrated to a kink profile. We can introduce the local coordinates n (perpendicular to the interface) and $\vec{a}$ (tangential to the interface), as shown in Figure 1.6. The corresponding increase in free energy is

$$\Delta G = \int d\vec{a} \int dn \left(\frac{d\psi_s}{dn}\right)^2$$
$$= \sigma \int d\vec{a}. \tag{1.77}$$

1.4.1.2 Equation of Motion for Interfaces and Growth Laws

Next, let us derive the Allen–Cahn equation of motion for the interfaces [32]. For this, we compute various terms in the TDGL equation 1.68 in terms of the interfacial coordinates $(n, \vec{a})$. We have

$$\vec{\nabla}\psi = \left.\frac{\partial\psi}{\partial n}\right|_t \hat{n}, \tag{1.78}$$

where $\hat{n}$ is the unit vector normal to the interface in the direction of increasing ψ. Further

$$\nabla^2\psi = \left.\frac{\partial^2\psi}{\partial n^2}\right|_t \hat{n}\cdot\hat{n} + \left.\frac{\partial\psi}{\partial n}\right|_t \vec{\nabla}\cdot\hat{n}. \tag{1.79}$$

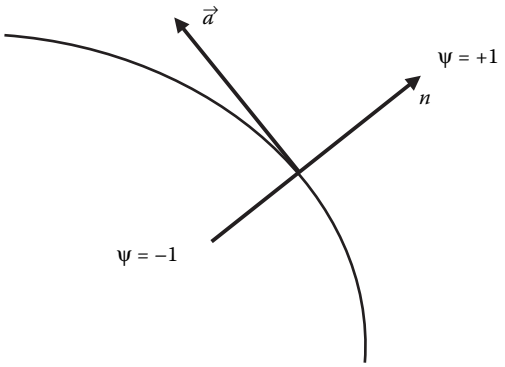

FIGURE 1.6 Curvilinear coordinates with reference to the interface. The normal coordinate is denoted as n and points from $\psi = -1$ to $\psi = +1$. The tangential coordinate points along the interface and is denoted as $\vec{a}$.

Finally, we use the identity

$$\left.\frac{\partial\psi}{\partial t}\right|_n \left.\frac{\partial t}{\partial n}\right|_\psi \left.\frac{\partial n}{\partial\psi}\right|_t = -1 \tag{1.80}$$

to obtain (from the TDGL equation)

$$\begin{aligned} -\left.\frac{\partial\psi}{\partial n}\right|_t \left.\frac{\partial n}{\partial t}\right|_\psi &= \psi - \psi^3 + \left.\frac{\partial^2\psi}{\partial n^2}\right|_t + \left.\frac{\partial\psi}{\partial n}\right|_t \vec{\nabla}\cdot\hat{n} \\ &\simeq \left.\frac{\partial\psi}{\partial n}\right|_t \vec{\nabla}\cdot\hat{n}. \end{aligned} \tag{1.81}$$

In the above simplification, we have used the fact that the interfaces are locally equilibrated to the static kink profile. We recognize that $\partial n/\partial t|_\psi = v(\vec{a})$, the normal interfacial velocity in the $\hat{n}$-direction. This yields the Allen–Cahn equation:

$$v(\vec{a}) = -\vec{\nabla}\cdot\hat{n} = -K(\vec{a}), \tag{1.82}$$

where K denotes the local curvature of the interface.

It is useful to examine the growth of a droplet of (say) $\psi = -1$ immersed in a matrix of $\psi = +1$. We consider the 3-d case of a spherical droplet with radius R. The normal unit vector at a point (x, y, z) on the surface of the sphere is

$$\hat{n} = \frac{x}{R}\hat{i} + \frac{y}{R}\hat{j} + \frac{z}{R}\hat{k}, \tag{1.83}$$

so that

$$\begin{aligned} \vec{\nabla}\cdot\hat{n} &= \frac{1}{R} - \frac{x^2}{R^3} + \frac{1}{R} - \frac{y^2}{R^3} + \frac{1}{R} - \frac{z^2}{R^3} \\ &= \frac{2}{R}. \end{aligned} \tag{1.84}$$

Further, $v(\vec{a}) = dR/dt$, and Equation 1.82 becomes

$$\frac{dR}{dt} = -\frac{2}{R}, \tag{1.85}$$

with the solution

$$R(0)^2 - R(t)^2 = 4t. \tag{1.86}$$

Thus, the droplet collapses on a timescale $t_c \sim R(0)^2$. In arbitrary dimensions d, the corresponding form of Equation 1.85 is

$$\frac{dR}{dt} = -\frac{d-1}{R}. \tag{1.87}$$

More generally, we can use Equation 1.82 to obtain the growth law for the domains in Figure 1.4. For a domain of characteristic size L, we have $v \sim dL/dt$ and curvature $K \sim 1/L$. This yields the diffusive growth law $L(t) \sim t^{1/2}$, which is valid for nonconserved scalar fields.

Before proceeding, it is important to consider the role of thermal fluctuations in the dynamics shown in Figure 1.4. It turns out that thermal noise is asymptotically irrelevant for ordering in systems that are free of disorder. This is because fluctuations only affect the interfacial profile. However, the fixed length scale of the interface becomes irrelevant in comparison with the diverging domain scale [33]. An equivalent argument is due to Bray [34,35], who used a renormalization-group (RG) approach to demonstrate that domain growth is driven by a fixed point at $T = 0$.

1.4.1.3 Correlation Function and Structure Factor

Now, if the system is characterized by a single length scale, the morphology of the domains does not change with time, apart from a scale factor. Therefore, the *order-parameter correlation function* exhibits a dynamical-scaling property [36]:

$$\begin{aligned} C(\vec{r},t) &\equiv \frac{1}{V}\int d\vec{R}\,\left[\langle\psi(\vec{R},t)\psi(\vec{R}+\vec{r},t)\rangle - \langle\psi(\vec{R},t)\rangle\langle\psi(\vec{R}+\vec{r},t)\rangle\right] \\ &= g\left(\frac{r}{L}\right), \end{aligned} \tag{1.88}$$

where V is the system volume, and the angular brackets denote an averaging over independent initial conditions and thermal fluctuations. This equal-time correlation function is a nonequilibrium quantity as domain growth is a nonequilibrium process. In Equation 1.88, $g(x)$ is a time-independent scaling function.

Actually, most experiments (e.g., neutron or light scattering) probe the time-dependent *structure factor*, which is the Fourier transform of the real-space correlation function:

$$S(\vec{k},t) = \int d\vec{r}\,e^{i\vec{k}\cdot\vec{r}}C(\vec{r},t), \tag{1.89}$$

where $\vec{k}$ is the wave-vector of the scattered beam. The corresponding dynamical-scaling form for $S(\vec{k}, t)$ is

$$S(\vec{k}, t) = L^d f(kL), \tag{1.90}$$

where $f(p)$ is a scaling function obtained as

$$f(p) = \int d\vec{x} e^{i\vec{p}\cdot\vec{x}} g(x). \tag{1.91}$$

The scaling functions $g(x)$ and $f(p)$ characterize the morphology of the ordering system. In experiments or simulations of domain growth, one usually attempts to obtain the functional forms of $g(x)$ and $f(p)$. Of course, a complete description of the morphology would require knowledge of all higher-order structure factors also, but these have limited experimental relevance.

The case with $d = 1$ does not obey these general arguments, and we discuss it separately here. For domain scales $L(t) \gg \xi_b$, there is only an exponentially decaying interaction of order e^{-L/ξ_b} between domain walls. This results in a logarithmic growth law $L(t) \sim \xi_b \ln t$. The corresponding scaling functions have been explicitly obtained by Nagai and Kawasaki [37].

1.4.1.4 Short-Distance Singularities and Porod's Law

Let us now discuss some general properties of the correlation function and the structure factor. The presence of sharp interfaces (defects) in the phase-ordering system results in a short-distance singularity of the correlation function. This can be obtained as follows. For simplicity, we first consider the 1-d case with a kink defect of size L. We are interested in short distances x such that $L \gg x \gg \xi_b$, where ξ_b is the correlation length. Therefore, we can approximate the kink defect by the sign-function:

$$\psi(x) = \mathrm{sgn}(x), \quad x \in \left[-\frac{L}{2}, \frac{L}{2}\right]. \tag{1.92}$$

The corresponding correlation function is obtained from Equation 1.88 as

$$\begin{aligned} C(x) &= \frac{1}{L}\int_{-L/2}^{L/2} d\bar{x}\ \mathrm{sgn}(\bar{x})\ \mathrm{sgn}(\bar{x}+x) \\ &= \frac{1}{L}\left[\int_0^{L/2} d\bar{x}\ \mathrm{sgn}(\bar{x}-x) + \int_0^{L/2} d\bar{x}\ \mathrm{sgn}(\bar{x}+x)\right] \\ &= 1 - \frac{2|x|}{L}. \end{aligned} \tag{1.93}$$

Notice that this function is non-analytic at $x = 0$. This short-distance singularity has important implications for the behavior of the structure factor at large wave-vectors. We will discuss this shortly, but let us first generalize the result in Equation 1.93 to arbitrary d.

We consider a d-dimensional kink with the interface located at $x = 0$. The order-parameter field is perfectly correlated in the $(d-1)$ dimensions that are perpendicular to x. Therefore, the correlation function at short distances is merely

$$C(\vec{r}) = 1 - \frac{2|x|}{L}, \tag{1.94}$$

where x now denotes the x-component of $\vec{r}$. In the isotropic case, the interface is randomly oriented in d-dimensional space. The corresponding correlation function is

$$C(\vec{r}) = 1 - \frac{2\langle|x|\rangle}{L}, \tag{1.95}$$

where $\langle\cdot\rangle$ denotes an average over the $(d-2)$ polar angles $\{\theta_1, \theta_2, \ldots, \theta_{d-2}\}$ and one azimuthal angle ϕ. This average is obtained as (using $x = r\sin\theta_1 \sin\theta_2 \ldots \sin\theta_{d-2}\cos\phi$)

$$\begin{aligned}\langle|x|\rangle &= \frac{\int_0^\pi d\theta_1 \sin^{d-2}\theta_1 \int_0^\pi d\theta_2 \sin^{d-3}\theta_2 \ldots \int_0^\pi d\theta_{d-2}\sin\theta_{d-2} \int_0^{2\pi} d\phi\; r\,|\sin\theta_1|\ldots|\sin\theta_{d-2}||\cos\phi|}{\int_0^\pi d\theta_1 \sin^{d-2}\theta_1 \int_0^\pi d\theta_2 \sin^{d-3}\theta_2 \ldots \int_0^\pi d\theta_{d-2}\sin\theta_{d-2}\int_0^{2\pi} d\phi} \\ &= r\,2^{d-2}B\left(\frac{d}{2},\frac{d}{2}\right)\cdot\frac{2}{\pi} \\ &= r\frac{1}{\sqrt{\pi}}\frac{\Gamma(d/2)}{\Gamma[(d+1)/2]}.\end{aligned} \tag{1.96}$$

In obtaining the above result, we have used the identities [38]

$$\begin{aligned}\int_0^{\pi/2} d\theta \sin^{n-1}\theta &= 2^{n-2}B\left(\frac{n}{2},\frac{n}{2}\right) \\ &= \frac{1}{2}B\left(\frac{1}{2},\frac{n}{2}\right),\end{aligned} \tag{1.97}$$

where $B(x, y)$ is the beta function

$$B(x,y) = \frac{\Gamma(x)\Gamma(y)}{\Gamma(x+y)}. \tag{1.98}$$

Putting the result for $\langle|x|\rangle$ into Equation 1.95, we obtain the short-distance behavior of the correlation function for interface defects in d dimensions:

$$C(r) = 1 - \frac{2}{\sqrt{\pi}}\frac{\Gamma(d/2)}{\Gamma[(d+1)/2]}\frac{r}{L}, \quad \frac{r}{L} \to 0. \tag{1.99}$$

The short-distance singularity in $C(r)$ as $r/L \to 0$ gives rise to a power-law decay of the structure-factor tail. Recall that the structure factor is merely the Fourier transform of the correlation function. From power-counting of the singular term in Equation 1.99, the functional form of the structure-factor tail is

$$S(k) = L^d \frac{A_d}{(kL)^{d+1}}, \quad kL \to \infty. \tag{1.100}$$

This important result is referred to as the Porod law and was first obtained for scattering from two-phase systems [39]. Notice that $S(k)$ satisfies the dynamical-scaling form in Equation 1.90. Here, A_d denotes the amplitude of the Porod tail, which can be extracted as follows. We have the inverse Fourier transform

$$\begin{aligned} C(r) &= \int \frac{d\vec{k}}{(2\pi)^d}\, e^{-i\vec{k}\cdot\vec{r}} S(k) \\ &= 1 - \int \frac{d\vec{k}}{(2\pi)^d} \left(1 - e^{-i\vec{k}\cdot\vec{r}}\right) S(k) \\ &= 1 - I(r), \end{aligned} \tag{1.101}$$

where we have used the fact that $C(0) = 1$.

We can decompose the above integral as

$$\begin{aligned} I(r) &= \int_0^K dk\, k^{d-1} \int \frac{d\Omega_k}{(2\pi)^d} \left(1 - e^{-i\vec{k}\cdot\vec{r}}\right) S(k) \\ &\quad + \int_K^\infty dk\, k^{d-1} \int \frac{d\Omega_k}{(2\pi)^d} \left(1 - e^{-i\vec{k}\cdot\vec{r}}\right) \frac{A_d}{Lk^{d+1}} \\ &= I_1(r) + I_2(r), \end{aligned} \tag{1.102}$$

where K is sufficiently large that the Porod tail applies for $k > K$. Finally, notice that we can extend the lower limit of $I_2(r)$ to $k = 0$. [This does not give rise to a divergence as $k \to 0$ because an extra factor of k^2 arises from the $(1 - e^{-\vec{k}\cdot\vec{r}})$ term.] Then

$$\begin{aligned} I(r) &= \int_0^K dk\, k^{d-1} \int \frac{d\Omega_k}{(2\pi)^d} \left(1 - e^{-i\vec{k}\cdot\vec{r}}\right) \left[S(k) - \frac{A_d}{Lk^{d+1}}\right] \\ &\quad + \int_0^\infty dk\, k^{d-1} \int \frac{d\Omega_k}{(2\pi)^d} \left(1 - e^{-i\vec{k}\cdot\vec{r}}\right) \frac{A_d}{Lk^{d+1}} \\ &= I_3(r) + I_4(r). \end{aligned} \tag{1.103}$$

Notice that $I_3(r)$ is analytic in r because of the finite upper limit of the k-integral. Clearly, the singular terms in $C(r)$ arise from $I_4(r)$, and we can isolate these as follows:

$$\begin{aligned} I_4(r) &= \frac{A_d}{L}\int_0^\infty \frac{d\vec{k}}{(2\pi)^d}\left(1-e^{-i\vec{k}\cdot\vec{r}}\right)\frac{1}{k^{d+1}} \\ &= \frac{A_d}{L}\int_0^\infty \frac{d\vec{k}}{(2\pi)^d}\left(1-e^{-i\vec{k}\cdot\vec{r}}\right)\int_0^\infty \frac{du}{\Gamma\left[(d+1)/2\right]}u^{((d+1)/2)-1}e^{-uk^2} \\ &= \frac{A_d}{L}\frac{1}{\Gamma\left[(d+1)/2\right]}\int_0^\infty du\, u^{(d-1)/2}\int_0^\infty \frac{d\vec{k}}{(2\pi)^d}\left(1-e^{-i\vec{k}\cdot\vec{r}}\right)e^{-uk^2} \\ &= \frac{A_d}{L}\frac{1}{(4\pi)^{d/2}\Gamma\left[(d+1)/2\right]}\int_0^\infty du\, u^{-1/2}\left(1-e^{-r^2/(4u)}\right). \end{aligned} \tag{1.104}$$

The final step is to evaluate the integral on the RHS. We make the substitution $z = r^2/(4u)$ to obtain

$$\begin{aligned} \int_0^\infty du\, u^{-1/2}\left(1-e^{-r^2/(4u)}\right) &= \frac{r}{2}\int_0^\infty dz\, z^{-3/2}\left(1-e^{-z}\right) \\ &= -\frac{r}{2}\,\Gamma\left(-\frac{1}{2}\right) \\ &= \sqrt{\pi}r. \end{aligned} \tag{1.105}$$

This yields the following expression for the singular part of $C(r)$:

$$C_s(r) = -A_d\frac{\sqrt{\pi}}{(4\pi)^{d/2}\Gamma\left[(d+1)/2\right]}\frac{r}{L}. \tag{1.106}$$

Comparing Equations 1.106 and 1.99, we obtain the exact amplitude of the Porod tail:

$$A_d = 2^{d+1}\pi^{(d/2)-1}\Gamma\left(\frac{d}{2}\right). \tag{1.107}$$

1.4.1.5 Ohta–Jasnow–Kawasaki Theory

Let us next consider the case with multiple defects or interfaces, corresponding to ordering from a random initial condition (see Figure 1.4). In this context, an approximate theory has been developed by Ohta et al. (OJK) [40]. Recall that the ordering system is described by an order parameter field $\psi(\vec{r},t)$ that obeys the TDGL equation 1.68. In the late stages of domain growth, the system consists of large domains with $\psi = +1$ or $\psi = -1$. The order parameter rapidly changes sign at the domain

boundaries. OJK introduced a nonlinear transformation $\psi \equiv \psi(m)$, where $m(\vec{r}, t)$ is an auxiliary field that varies smoothly through the interface. The simplest choice for m is the normal distance from the interface, so that $m(\vec{r}, t) = 0$ on the interface. The corresponding choice for the nonlinear transformation is then $\psi = \text{sgn}(m)$. Let us obtain the equation obeyed by $m(\vec{r}, t)$ as follows. Recall the Allen–Cahn equation $v(\vec{a}) = -\vec{\nabla} \cdot \hat{n}$, where $\hat{n}$ is the unit vector normal to the interface. We use the fact that

$$\hat{n} = \frac{\vec{\nabla} m}{|\vec{\nabla} m|} \tag{1.108}$$

to obtain

$$v = -\vec{\nabla} \cdot \hat{n} = -\frac{\nabla^2 m}{|\vec{\nabla} m|} + \frac{n_i n_j \nabla_i \nabla_j m}{|\vec{\nabla} m|}. \tag{1.109}$$

Further, in a reference frame moving with the interface,

$$\frac{dm}{dt} = \frac{\partial m}{\partial t} + \vec{\nabla} m \cdot \vec{v} = 0. \tag{1.110}$$

We use $\vec{\nabla} m \cdot \vec{v} = |\vec{\nabla} m| v$ to obtain

$$v = -\frac{1}{|\vec{\nabla} m|} \frac{\partial m}{\partial t}. \tag{1.111}$$

Comparing Equations 1.109 and 1.111, we obtain the required equation for $m(\vec{r}, t)$:

$$\frac{\partial}{\partial t} m(\vec{r}, t) = \nabla^2 m - n_i n_j \nabla_i \nabla_j m. \tag{1.112}$$

Equation 1.112 is nonlinear and analytically intractable, as was the case with the original TDGL equation. Then, OJK replaced the term $n_i n_j$ by its spherical average as

$$n_i n_j \simeq \frac{\delta_{ij}}{d}. \tag{1.113}$$

Under this approximation, the auxiliary field $m(\vec{r}, t)$ obeys the diffusion equation:

$$\frac{\partial}{\partial t} m(\vec{r}, t) = \left(\frac{d-1}{d} \right) \nabla^2 m \equiv D \nabla^2 m. \tag{1.114}$$

Now, we are in a position to calculate the correlation function of the ψ-field from the correlation function of the m-field. We model the random initial condition for the field $m(\vec{r}, 0)$ by a Gaussian distribution with zero mean and correlation

$$\left\langle m(\vec{r}, 0) m(\vec{r}', 0) \right\rangle = A \delta(\vec{r} - \vec{r}'). \tag{1.115}$$

The appropriate distribution is

$$P\left[m(\vec{r},0)\right] = \frac{1}{\sqrt{2\pi\sigma(0)^2}} \exp\left[-\frac{m(\vec{r},0)^2}{2\sigma(0)^2}\right], \quad \sigma(0)^2 = \left\langle m(\vec{r},0)^2 \right\rangle. \tag{1.116}$$

As the evolution of $m(\vec{r},t)$ is governed by the linear equation 1.114, the distribution of m remains Gaussian for all times:

$$P\left[m(\vec{r},t)\right] = \frac{1}{\sqrt{2\pi\sigma(t)^2}} \exp\left[-\frac{m(\vec{r},t)^2}{2\sigma(t)^2}\right], \quad \sigma(t)^2 = \left\langle m(\vec{r},t)^2 \right\rangle. \tag{1.117}$$

Let us calculate the general correlation function (at unequal space-time points)

$$\begin{aligned} C(\vec{r}_1,t_1;\vec{r}_2,t_2) &= \langle \psi(\vec{r}_1,t_1)\psi(\vec{r}_2,t_2)\rangle \\ &= \left\langle \operatorname{sgn}\left[m(\vec{r}_1,t_1)\right] \operatorname{sgn}\left[m(\vec{r}_2,t_2)\right]\right\rangle. \end{aligned} \tag{1.118}$$

To obtain this average, we need the normalized bivariate Gaussian distribution for $m(\vec{r}_1,t_1)$ $(=x$, say) and $m(\vec{r}_2,t_2)$ $(=y)$:

$$\begin{aligned} P(x,y) = &\frac{1}{2\pi\sigma(t_1)\sigma(t_2)\sqrt{1-\gamma^2}} \\ &\times \exp\left[-\frac{1}{2(1-\gamma^2)}\left(\frac{x^2}{\sigma(t_1)^2} + \frac{y^2}{\sigma(t_2)^2} - \frac{2\gamma xy}{\sigma(t_1)\sigma(t_2)}\right)\right], \end{aligned} \tag{1.119}$$

where

$$\begin{aligned} \sigma(t_1)^2 &= \langle x^2\rangle = \langle m(\vec{r}_1,t_1)^2\rangle, \\ \sigma(t_2)^2 &= \langle y^2\rangle = \langle m(\vec{r}_2,t_2)^2\rangle, \\ \gamma &= \frac{\langle xy\rangle}{\sqrt{\langle x^2\rangle\langle y^2\rangle}} = \frac{\langle m(\vec{r}_1,t_1)m(\vec{r}_2,t_2)\rangle}{\sqrt{\langle m(\vec{r}_1,t_1)^2\rangle\langle m(\vec{r}_2,t_2)^2\rangle}}. \end{aligned} \tag{1.120}$$

We will calculate the quantities $\sigma(t_1), \sigma(t_2)$ and γ shortly. Let us first obtain the correlation function

$$\begin{aligned} C(\vec{r}_1,t_1;\vec{r}_2,t_2) = &\frac{1}{2\pi\sigma(t_1)\sigma(t_2)\sqrt{1-\gamma^2}} \int_{-\infty}^{\infty} dx \int_{-\infty}^{\infty} dy \frac{x}{\sqrt{x^2}} \frac{y}{\sqrt{y^2}} \\ &\times \exp\left[-\frac{1}{2(1-\gamma^2)}\left(\frac{x^2}{\sigma(t_1)^2} + \frac{y^2}{\sigma(t_2)^2} - \frac{2\gamma xy}{\sigma(t_1)\sigma(t_2)}\right)\right], \end{aligned} \tag{1.121}$$

where we have used $\mathrm{sgn}(z) = z/\sqrt{z^2}$. We rescale as $x' = x/\sigma(t_1)$ and $y' = y/\sigma(t_2)$ to obtain (dropping the primes)

$$C(\vec{r}_1, t_1; \vec{r}_2, t_2) = \frac{1}{2\pi\sqrt{1-\gamma^2}} \int_{-\infty}^{\infty} dx \int_{-\infty}^{\infty} dy \frac{x}{\sqrt{x^2}} \frac{y}{\sqrt{y^2}} \exp\left(-\alpha x^2 - \alpha y^2 + \beta xy\right), \tag{1.122}$$

where

$$\alpha = \frac{1}{2(1-\gamma^2)},$$
$$\beta = \frac{\gamma}{(1-\gamma^2)}. \tag{1.123}$$

The integral on the RHS of Equation 1.122 can be simplified by using the identity

$$\frac{1}{\sqrt{z}} = \frac{1}{\sqrt{\pi}} \int_{-\infty}^{\infty} d\theta \exp(-z\theta^2). \tag{1.124}$$

This yields

$$\begin{aligned} C(\vec{r}_1, t_1; \vec{r}_2, t_2) &= \frac{1}{2\pi^2\sqrt{1-\gamma^2}} \int_{-\infty}^{\infty} d\theta \int_{-\infty}^{\infty} d\phi \int_{-\infty}^{\infty} dx \int_{-\infty}^{\infty} dy\, xy \\ &\quad \times \exp\left[-(\alpha+\theta^2)x^2 - (\alpha+\phi^2)y^2 + \beta xy\right] \\ &= \frac{1}{2\pi^2\sqrt{1-\gamma^2}} \frac{\partial}{\partial\beta} \int_{-\infty}^{\infty} d\theta \int_{-\infty}^{\infty} d\phi \int_{-\infty}^{\infty} dx \int_{-\infty}^{\infty} dy \\ &\quad \times \exp\left[-(\alpha+\theta^2)x^2 - (\alpha+\phi^2)y^2 + \beta xy\right]. \end{aligned} \tag{1.125}$$

The integrals over x and y are performed using the general expression for the Gaussian integral:

$$\int_{-\infty}^{\infty} dz \exp(-p^2 z^2 \pm qz) = \exp\left(\frac{q^2}{4p^2}\right) \frac{\sqrt{\pi}}{|p|}. \tag{1.126}$$

Then, the integrand becomes

$$\begin{aligned} h(\theta, \phi) &= \int_{-\infty}^{\infty} dx \exp\left[-(\alpha+\theta^2)x^2\right] \int_{-\infty}^{\infty} dy \exp\left[-(\alpha+\phi^2)y^2 + \beta xy\right] \\ &= \int_{-\infty}^{\infty} dx \exp\left[-(\alpha+\theta^2)x^2\right] \exp\left[\frac{\beta^2 x^2}{4(\alpha+\phi^2)}\right] \sqrt{\frac{\pi}{\alpha+\phi^2}} \\ &= \sqrt{\frac{\pi}{\alpha+\phi^2}} \int_{-\infty}^{\infty} dx \exp\left[-\left(\alpha+\theta^2 - \frac{\beta^2}{4(\alpha+\phi^2)}\right)x^2\right] \end{aligned}$$

$$= \sqrt{\frac{\pi}{\alpha+\phi^2}} \frac{\sqrt{\pi}}{\left[\alpha+\theta^2-\dfrac{\beta^2}{4(\alpha+\phi^2)}\right]^{1/2}}. \tag{1.127}$$

Notice that the x-integral is well defined because

$$\alpha+\theta^2-\frac{\beta^2}{4(\alpha+\phi^2)} > \alpha-\frac{\beta^2}{4\alpha} > 0. \tag{1.128}$$

Finally, we have

$$\begin{aligned} C(\vec{r}_1,t_1;\vec{r}_2,t_2) &= \frac{\beta}{8\pi\sqrt{1-\gamma^2}} \int_{-\infty}^{\infty} d\theta \int_{-\infty}^{\infty} d\phi \, \frac{1}{\left[\alpha+\phi^2\right]^{3/2}} \frac{1}{\left[\alpha+\theta^2-\dfrac{\beta^2}{4(\alpha+\phi^2)}\right]^{3/2}} \\ &= \frac{\beta}{4\pi\sqrt{1-\gamma^2}} \int_{-\infty}^{\infty} d\phi \frac{1}{(\alpha+\phi^2)^{3/2}} \frac{1}{\left[\alpha-\dfrac{\beta^2}{4(\alpha+\phi^2)}\right]} \\ &= \frac{\beta}{\pi\sqrt{1-\gamma^2}} \int_{-\infty}^{\infty} d\phi \frac{1}{(\alpha+\phi^2)^{1/2}} \frac{1}{\left(4\alpha\phi^2+4\alpha^2-\beta^2\right)}. \end{aligned} \tag{1.129}$$

Some further algebra yields the final result:

$$C(\vec{r}_1,t_1;\vec{r}_2,t_2) = \frac{2}{\pi}\sin^{-1}(\gamma), \tag{1.130}$$

where γ was defined in Equation 1.120.

Our only remaining task is to obtain the quantity γ, which is the (normalized) correlation function of the auxiliary field $m(\vec{r},t)$. It is easy to calculate this quantity in momentum space as follows. We note that

$$\begin{aligned} m(\vec{r},t) &= e^{Dt\nabla^2} m(\vec{r},0), \\ m(\vec{k},t) &= e^{-Dtk^2} m(\vec{k},0). \end{aligned} \tag{1.131}$$

Further, we have

$$\begin{aligned} \left\langle m(\vec{k},0)m(\vec{k}',0)\right\rangle &= \int d\vec{r} e^{i\vec{k}\cdot\vec{r}} \int d\vec{r}' e^{i\vec{k}'\cdot\vec{r}'} \left\langle m(\vec{r},0)m(\vec{r}',0)\right\rangle \\ &= A\int d\vec{r} e^{i(\vec{k}+\vec{k}')\cdot\vec{r}} = A\delta(\vec{k}+\vec{k}'), \end{aligned} \tag{1.132}$$

where we have used Equation 1.115. Therefore

$$\begin{aligned} \left\langle m(\vec{k}_1,t_1)m(\vec{k}_2,t_2)\right\rangle &= e^{-Dt_1k_1^2} e^{-Dt_2k_2^2} \left\langle m(\vec{k}_1,0)m(\vec{k}_2,0)\right\rangle \\ &= A\delta(\vec{k}_1+\vec{k}_2) e^{-D(t_1k_1^2+t_2k_2^2)}. \end{aligned} \tag{1.133}$$

Finally, we obtain

$$\begin{aligned}\langle m(\vec{r}_1,t_1)m(\vec{r}_2,t_2)\rangle &= \int \frac{d\vec{k}_1}{(2\pi)^d} e^{-i\vec{k}_1\cdot\vec{r}_1} \int \frac{d\vec{k}_2}{(2\pi)^d} e^{-i\vec{k}_2\cdot\vec{r}_2} \left\langle m(\vec{k}_1,t_1)m(\vec{k}_2,t_2)\right\rangle \\ &= A\int \frac{d\vec{k}_1}{(2\pi)^d} e^{-i\vec{k}_1\cdot(\vec{r}_1-\vec{r}_2)} e^{-D(t_1+t_2)k_1^2} \\ &= \frac{A}{[4\pi D(t_1+t_2)]^{d/2}} \exp\left[-\frac{r^2}{4D(t_1+t_2)}\right], \end{aligned} \tag{1.134}$$

where $\vec{r} = \vec{r}_1 - \vec{r}_2$. Thus

$$\begin{aligned}\gamma &= \frac{\langle m(\vec{r}_1,t_1)m(\vec{r}_2,t_2)\rangle}{\sqrt{\left\langle m(\vec{r}_1,t_1)^2\right\rangle \left\langle m(\vec{r}_2,t_2)^2\right\rangle}} \\ &= \left(\frac{2\sqrt{t_1 t_2}}{t_1+t_2}\right)^{d/2} \exp\left[-\frac{r^2}{4D(t_1+t_2)}\right]. \end{aligned} \tag{1.135}$$

Equations 1.130 and 1.135 constitute the OJK result for the correlation function (at unequal space-time points) for the nonconserved ordering problem.

1.4.1.6 Implications of the OJK Function

We are usually interested in the equal-time correlation function ($\vec{r} = \vec{r}_1 - \vec{r}_2$)

$$\begin{aligned} C(\vec{r},t) &\equiv C(\vec{r}_1,t;\vec{r}_2,t) \\ &= \frac{2}{\pi}\sin^{-1}\left[\exp\left(-\frac{r^2}{8Dt}\right)\right]. \end{aligned} \tag{1.136}$$

Notice that the OJK result has the scaling form in Equation 1.88 with the domain scale $L(t) \sim (8Dt)^{1/2}$. This confirms the result we had obtained from dimensional analysis of the Allen–Cahn equation. Further, the OJK function is in excellent agreement with results obtained from experiments and numerical simulations. In Figure 1.7a, we show numerical results for the correlation function of the ordering ferromagnet in Figure 1.4. We plot $C(r,t)$ versus r/L at different times—the resultant data collapse confirms the scaling form in Equation 1.88. The OJK function is also plotted in Figure 1.7a. In Figure 1.7b, we show numerical data for the scaled structure factor, $L^{-d}S(k,t)$ versus kL, at different times. Again, the data collapses onto a scaling function, in accordance with the scaling form in Equation 1.90. The tail of the structure factor decays as a power law, $S(k,t) \sim k^{-(d+1)}$, which is the Porod tail in Equation 1.100. In Figure 1.7b, we also plot the Fourier transform of the OJK function. As expected, this also shows a Porod tail. Our next task is to demonstrate this explicitly. Before

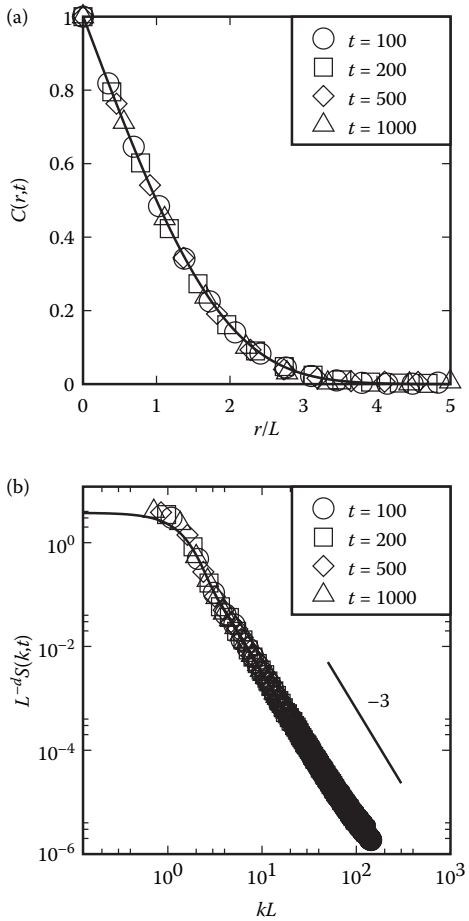

FIGURE 1.7 (a) Scaled correlation function [$C(r,t)$ versus r/L] for the evolution depicted in Figure 1.4. The numerical data is obtained as an average over 5 independent runs for systems of size 1024^2. The length scale $L(t)$ is defined as the distance over which the correlation function falls to half its maximum value. We show data for times 100, 200, 500, 1000—denoted by the specified symbols. The solid line denotes the OJK function in Equations 1.130 and 1.135, scaled in the same manner as the numerical data. (b) Scaled structure factor [$L^{-d}S(k,t)$ versus kL], corresponding to the data in (a). In this case, we plot the data on a log-log scale. The solid line denotes the Fourier transform of the OJK function. The line with slope -3 corresponds to the Porod tail.

doing that, we present data for the domain growth law [$L(t)$ versus t] in Figure 1.8. We see that the domain-growth process obeys the Allen–Cahn law, $L(t) \sim t^{1/2}$.

In our earlier discussion, we had stressed that the short-distance singularities of the correlation function lead to a power-law decay of the structure factor. In this context, it is useful to undertake a short-distance expansion of the OJK function. We identify

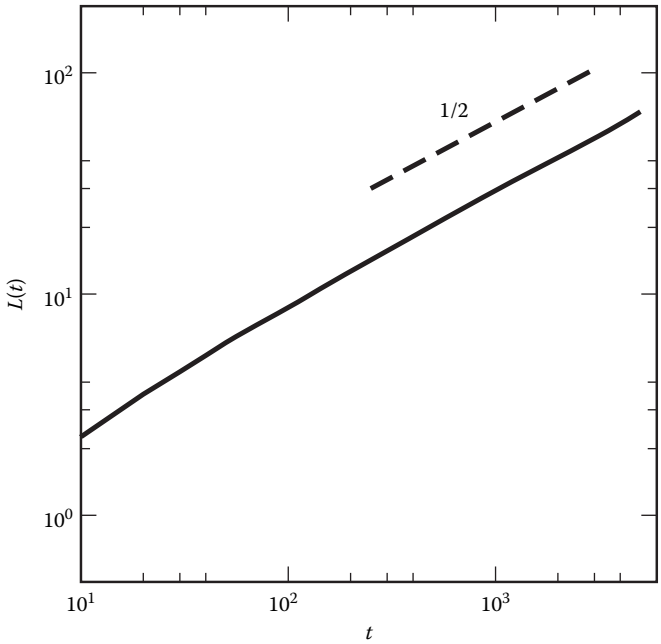

FIGURE 1.8 Domain growth law for the evolution depicted in Figure 1.4. The numerical details are the same as in Figure 1.7. We plot the data on a log-log scale. The dashed line denotes the Allen–Cahn growth law, $L(t) \sim t^{1/2}$.

the scaled variable $x = r/L$, and consider the function

$$g(x) = \frac{2}{\pi} \sin^{-1}\left(e^{-x^2}\right). \tag{1.137}$$

In the limit $x \to 0$, we have $\gamma = e^{-x^2} \to 1$. For a small-x expansion of $g(x)$, it is convenient to use the identity [38]

$$\sin^{-1}\gamma = \gamma F\left(\frac{1}{2}, \frac{1}{2}; \frac{3}{2}; \gamma^2\right), \tag{1.138}$$

where we have introduced the hypergeometric function

$$F(a, b; c; z) = \sum_{n=0}^{\infty} \frac{\Gamma(a+n)\Gamma(b+n)}{\Gamma(c+n)\, n!} \frac{\Gamma(c)}{\Gamma(a)\Gamma(b)}\, z^n. \tag{1.139}$$

The hypergeometric function satisfies the relation [38]:

$$\begin{aligned} F(a, b; c; z) = {} & \frac{\Gamma(c)\Gamma(c-a-b)}{\Gamma(c-a)\Gamma(c-b)} F(a, b; a+b-c+1; 1-z) + (1-z)^{c-a-b} \\ & \times \frac{\Gamma(c)\Gamma(a+b-c)}{\Gamma(a)\Gamma(b)} F(c-a, c-b; c-a-b+1; 1-z). \end{aligned} \tag{1.140}$$

Using this relation, we have

$$\sin^{-1}\gamma = \frac{\pi}{2}\gamma F\left(\frac{1}{2},\frac{1}{2};\frac{1}{2};1-\gamma^2\right) - \gamma(1-\gamma^2)^{1/2}F\left(1,1;\frac{3}{2};1-\gamma^2\right) \quad (1.141)$$

and

$$g(x) = e^{-x^2}F\left(\frac{1}{2},\frac{1}{2};\frac{1}{2};1-e^{-2x^2}\right) - \frac{2}{\pi}e^{-x^2}\left(1-e^{-2x^2}\right)^{1/2}F\left(1,1;\frac{3}{2};1-e^{-2x^2}\right)$$
$$\equiv A(x) + B(x). \quad (1.142)$$

The singular terms for $x \to 0$ arise only from the second term (B) on the RHS of Equation 1.142. The first few of these are obtained as

$$B(x) = -\frac{2\sqrt{2}}{\pi}x + \frac{\sqrt{2}}{3\pi}x^3 + O(x^5). \quad (1.143)$$

The first term (A) yields only analytic terms for $x \to 0$. Some calculation shows that the $O(x^2)$ term is missing in the expansion of A, and

$$A(x) = 1 - O(x^4). \quad (1.144)$$

Thus, the overall result for $g(x)$ is

$$g(x) = 1 - \frac{2\sqrt{2}}{\pi}x + \frac{\sqrt{2}}{3\pi}x^3 + O(x^4). \quad (1.145)$$

As before, the linear term in x gives rise to the Porod tail

$$S(k) = L^d\frac{A_{\mathrm{OJK}}}{(kL)^{d+1}}, \quad kL \to \infty. \quad (1.146)$$

From Equations 1.106 and 1.143, we observe that

$$A_{\mathrm{OJK}}\frac{\sqrt{\pi}}{(4\pi)^{d/2}\Gamma\left(\frac{d+1}{2}\right)} = \frac{2\sqrt{2}}{\pi}, \quad (1.147)$$

so that

$$A_{\mathrm{OJK}} = 2^{d+3/2}\pi^{(d-3)/2}\Gamma\left(\frac{d+1}{2}\right). \quad (1.148)$$

The absence of the x^2-term in the expansion of $g(x)$ also has an important consequence for the structure factor. In the limit $x \to 0$, we have

$$\lim_{x\to 0}\nabla^2 g(x) = \lim_{x\to 0}\left(\frac{d^2g}{dx^2} + \frac{d-1}{x}\frac{dg}{dx}\right)$$
$$= \lim_{x\to 0} -\frac{2\sqrt{2}(d-1)}{\pi x}. \quad (1.149)$$

We can rewrite $\nabla^2 g$ as

$$\nabla^2 g(x) = \nabla^2 \int \frac{d\vec{p}}{(2\pi)^d} e^{-i\vec{p}\cdot\vec{x}} f(p) = -\int \frac{d\vec{p}}{(2\pi)^d} e^{-i\vec{p}\cdot\vec{x}} p^2 f(p), \tag{1.150}$$

where $\vec{p} = \vec{k}L$ and $f(p)$ is the scaling function for the structure factor—see Equation 1.90.

Further, we have the identity

$$\frac{1}{x} = \int \frac{d\vec{p}}{(2\pi)^d} e^{-i\vec{p}\cdot\vec{x}} \frac{2^{d-1}\pi^{(d-1)/2}\Gamma\left[(d-1)/2\right]}{p^{d-1}}. \tag{1.151}$$

Therefore, Equation 1.150 can be rewritten as

$$\int \frac{d\vec{p}}{(2\pi)^d} \left[p^2 f(p) - \frac{2^{d-1}\pi^{(d-1)/2}\Gamma\left[(d-1)/2\right] 2\sqrt{2}(d-1)}{\pi p^{d-1}} \right] = 0, \tag{1.152}$$

or

$$\int_0^\infty dp \left[p^{d+1} f(p) - 2^{d+3/2}\pi^{(d-3)/2}\Gamma\left(\frac{d+1}{2}\right) \right] = 0. \tag{1.153}$$

This reconfirms the result in Equations 1.146 and 1.148, viz.,

$$f(p) = \frac{2^{d+3/2}\pi^{(d-3)/2}\Gamma\left[(d+1)/2\right]}{p^{d+1}}, \quad p \to \infty. \tag{1.154}$$

Further, Equation 1.153 constitutes a sum rule that must be obeyed by the scaling function. This is referred to as Tomita's sum rule [41,42].

An important extension of the OJK result is due to Oono and Puri (OP) [43], who incorporated the effects of non-zero interfacial thickness into the analytical form for the correlation function. This extension was of considerable experimental and numerical relevance because the non-zero interfacial thickness has a severe impact on the tail of the structure factor. In particular, the power-law decay is replaced by a Gaussian decay for finite times, and the Porod tail is only recovered for $t \to \infty$.

1.4.1.7 Kawasaki–Yalabik–Gunton Theory

An alternative approach to the nonconserved ordering problem is due to Kawasaki et al. (KYG) [44]. The KYG theory yields the same result for the correlation function as does OJK theory. As before, we require an approximate solution to the TDGL Equation 1.68, which we reproduce here for convenience:

$$\frac{\partial}{\partial t}\psi(\vec{r},t) = \psi - \psi^3 + \nabla^2\psi.$$

Let us consider the Fourier transform of the TDGL equation:

$$\frac{\partial}{\partial t}\psi(\vec{k},t) = (1-k^2)\psi(\vec{k},t) - \int \frac{d\vec{k}_1}{(2\pi)^d}\int \frac{d\vec{k}_2}{(2\pi)^d}\int \frac{d\vec{k}_3}{(2\pi)^d}\delta(\vec{k}-\vec{k}_1-\vec{k}_2-\vec{k}_3) \times \psi(\vec{k}_1,t)\psi(\vec{k}_2,t)\psi(\vec{k}_3,t). \tag{1.155}$$

The linear part of Equation 1.155 is

$$\frac{\partial}{\partial t}m(\vec{k},t) = (1-k^2)m(\vec{k},t), \tag{1.156}$$

with the solution:

$$m(\vec{k},t) = e^{\gamma(\vec{k})t}m(\vec{k},0), \quad \gamma(\vec{k}) = 1-k^2. \tag{1.157}$$

The formal solution of the nonlinear equation 1.155 is

$$\psi(\vec{k},t) = m(\vec{k},t) - \int_0^t dt' e^{\gamma(\vec{k})(t-t')}\int \frac{d\vec{k}_1}{(2\pi)^d}\int \frac{d\vec{k}_2}{(2\pi)^d}\int \frac{d\vec{k}_3}{(2\pi)^d} \times \delta(\vec{k}-\vec{k}_1-\vec{k}_2-\vec{k}_3)\psi(\vec{k}_1,t')\psi(\vec{k}_2,t')\psi(\vec{k}_3,t'). \tag{1.158}$$

KYG solved this integral equation iteratively, using the linear solution $m(\vec{k},t)$ to obtain an expansion in integrals of products of $m(\vec{k},t)$. Notice that $m(\vec{k},t)$ diverges with time, so each term of this expansion also diverges in time. KYG used a technique developed by Suzuki [45,46] to perform a partial resummation of the terms in this expansion to obtain a well-controlled result:

$$\psi(\vec{r},t) \simeq \frac{m(\vec{r},t)}{\sqrt{1+m(\vec{r},t)^2}}. \tag{1.159}$$

In the large-t limit, $m(\vec{r},t)$ is very large and

$$\psi(\vec{r},t) \simeq \operatorname{sgn}\left[m(\vec{r},t)\right]. \tag{1.160}$$

Notice that this is identical to the nonlinear transformation in OJK theory. In this case also, the auxiliary field $m(\vec{r},t)$ obeys the diffusion equation ($D=1$ here), with the only difference being that there is an additional factor of e^t:

$$m(\vec{r},t) = e^{t(1+\nabla^2)}m(\vec{r},0). \tag{1.161}$$

We assume that $m(\vec{r},0)$ has a Gaussian distribution (cf. Equation 1.116), so that $m(\vec{r},t)$ is also described by a Gaussian distribution. The calculation of the correlation function for the field $\psi(\vec{r},t)$ is identical to that described for OJK theory. The final result is again the OJK function in Equations 1.130 and 1.135 with $D=1$.

Finally, it is useful to examine the KYG theory from an alternative perspective. Let us consider the nonlinear transformation

$$\psi(\vec{r},t) = \frac{m(\vec{r},t)}{\sqrt{1+m(\vec{r},t)^2}} \tag{1.162}$$

and determine the equation that is satisfied by $m(\vec{r},t)$. Some simple algebra yields the relevant equation, which is

$$\frac{\partial}{\partial t}m(\vec{r},t) = m + \nabla^2 m - \frac{3m|\vec{\nabla}m|^2}{1+m^2}. \tag{1.163}$$

Thus, the KYG approximation is equivalent to discarding the nonlinear term on the RHS of Equation 1.163. There is no justification for such an approximation, so the KYG theory only constitutes an approximate solution to the ordering problem. This can be explicitly demonstrated by comparing the evolution profiles obtained from Equation 1.159 with those obtained numerically from the original TDGL equation. In a sense, it is fortunate that the nonlinear transformation in Equation 1.159 faithfully mimics the actual defect statistics, thereby yielding excellent results for statistical quantities like the correlation function and the structure factor.

In the next subsection, we will see that the KYG "solution" in Equation 1.159 readily generalizes to the problem of domain growth in a system described by a vector order parameter.

1.4.2 Case with Vector Order Parameter

The vector version of the TDGL equation, where ψ is replaced by an n-component vector $\vec{\psi} = (\psi_1, \psi_2, \ldots \psi_n)$, is also of great experimental relevance. In dimensionless units, this has the following form for $T < T_c$ and $\vec{h} = 0$:

$$\frac{\partial}{\partial t}\vec{\psi}(\vec{r},t) = \vec{\psi} - |\vec{\psi}|^2\vec{\psi} + \nabla^2\vec{\psi} + \vec{\theta}(\vec{r},t), \tag{1.164}$$

where the vector noise $\vec{\theta}(\vec{r},t)$ satisfies

$$\begin{aligned} \overline{\vec{\theta}(\vec{r},t)} &= 0, \\ \overline{\theta_i(\vec{r}',t')\theta_j(\vec{r}'',t'')} &= 2\epsilon\delta_{ij}\delta(\vec{r}'-\vec{r}'')\delta(t'-t''). \end{aligned} \tag{1.165}$$

For example, the $n = 2$ case (XY model) is relevant in the ordering of superconductors, superfluids, and liquid crystals. Figure 1.9 shows the evolution of the vector field (ψ_1, ψ_2) for the $d = 2$ XY model from a disordered initial condition. In this case, the topological defects are vortices and anti-vortices, and domain growth is driven by the

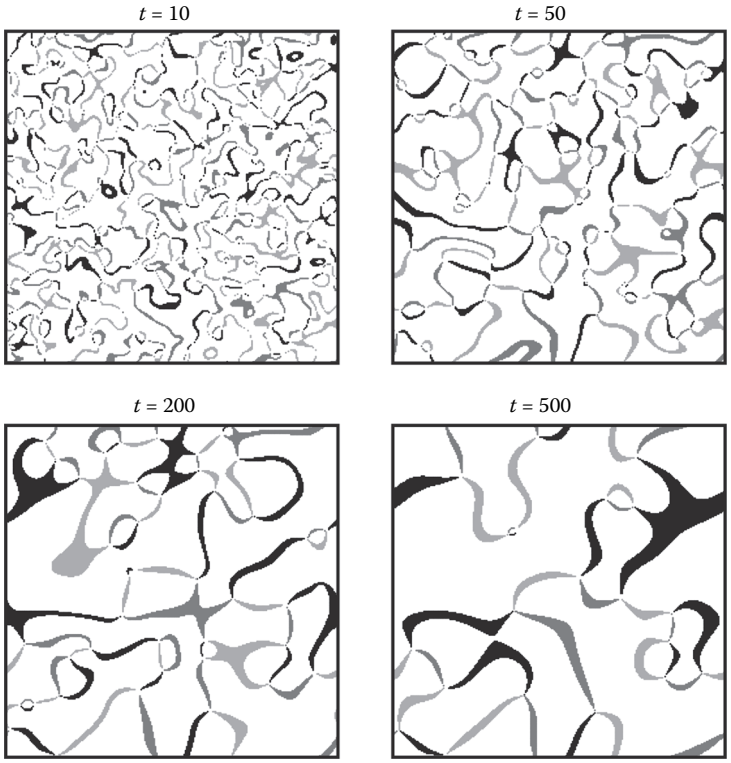

FIGURE 1.9 (See color insert following page xxx.) Evolution of the dimensionless XY model from a disordered initial condition. The pictures were obtained from a Euler-discretized version of Equation 1.164 with $n = 2$ and $\epsilon = 0$. The numerical details are the same as for Figure 1.4. The snapshots show regions of constant phase $\theta_\psi = \tan^{-1}(\psi_2/\psi_1)$, measured in radians, with the following color coding: $\theta_\psi \in [1.85, 2.15]$ (black); $\theta_\psi \in [3.85, 4.15]$ (red); $\theta_\psi \in [5.85, 6.15]$ (green). Typically, a meeting point of the three colors denotes a vortex defect.

annihilation of these defects. The $n = 3$ case (Heisenberg model) is also of relevance in the ordering of liquid crystals and in the evolution dynamics of the early universe.

1.4.2.1 Generalized Porod's Law

As before, the nature of defects in the ordering system determines general properties of the correlation function and the structure factor. The presence of n-component defects (e.g., vortices for $n = 2, d = 2$; vortex lines for $n = 2, d = 3$; monopoles for $n = 3, d = 3$; etc.) again yields a power-law or *generalized Porod* tail for the scaled structure factor [47,48], that is,

$$f(p) \sim p^{-(d+n)}, \quad p \to \infty. \tag{1.166}$$

The corresponding exact result for the singular behavior of the scaled correlation function of a single defect at short distances is as follows [49]:

$$g(x) = 1 + \pi^{(n-2)/2} \frac{\Gamma(d/2)\,\Gamma[(n+1)/2]^2\,\Gamma(-n/2)}{\Gamma[(d+n)/2)]\,\Gamma(n/2)} x^n + \text{higher-order terms.} \tag{1.167}$$

This result is obtained by a generalization (to the n-component case) of the arguments that resulted in Equation 1.99. That result was obtained for interface defects and corresponds to the $n = 1$ case of Equation 1.167. The singular behavior for even values of n has to be carefully extracted from the above expression and involves logarithmic corrections as $1 - g(x) \sim x^n \ln x$. Furthermore, there is no analog of the Tomita sum rule for the vector-ordering problem.

1.4.2.2 Bray–Puri–Toyoki Theory

Bray and Puri (BP) [47] and (independently) Toyoki (T) [48] used a defect-dynamics approach to obtain an approximate solution for the correlation function of the n-component TDGL equation in d-dimensional space. The BPT result is valid for $n \leq d$, corresponding to the case where topological defects are present. The starting point of the BP calculation is a generalization of the KYG solution for the scalar TDGL equation in Equation 1.159 [50]:

$$\vec{\psi}(\vec{r}, t) \simeq \frac{\vec{m}(\vec{r}, t)}{\sqrt{1 + \sum_{i=1}^{n} m_i(\vec{r}, t)^2}}. \tag{1.168}$$

Here, $\vec{m}(\vec{r}, t)$ is the solution of the linear equation (cf. Equation 1.156)

$$\frac{\partial}{\partial t}\vec{m}(\vec{r}, t) = \vec{m} + \nabla^2 \vec{m}, \tag{1.169}$$

so that

$$\vec{m}(\vec{r}, t) = e^{t(1+\nabla^2)}\vec{m}(\vec{r}, 0). \tag{1.170}$$

In the large-t limit, $\vec{m}(\vec{r}, t)$ is very large and

$$\vec{\psi}(\vec{r}, t) \simeq \frac{\vec{m}(\vec{r}, t)}{|\vec{m}(r, t)|}. \tag{1.171}$$

The subsequent calculation is analogous to that described in Equation 1.116 onwards. BP obtained an explicit scaling form for the correlation function:

$$\begin{aligned} C(\vec{r}, t) &= \langle \vec{\psi}(\vec{r}_1, t) \cdot \vec{\psi}(\vec{r}_2, t) \rangle \\ &= \frac{n\gamma}{2\pi} \left[B\left(\frac{n+1}{2}, \frac{1}{2}\right) \right]^2 F\left(\frac{1}{2}, \frac{1}{2}; \frac{n+2}{2}; \gamma^2\right), \end{aligned} \tag{1.172}$$

where $\gamma = \exp(-r^2/L^2)$, L being the average defect length-scale. BP demonstrated that the length scale obeys the Allen–Cahn growth law, $L(t) \sim t^{1/2}$. (A more careful calculation demonstrates that there are logarithmic corrections when $n = d = 2$, and $L(t) \sim (t/\ln t)^{1/2}$ [51].) As in the case of the OJK function, Equation 1.172 is valid when the defect core size is identically zero. The nonzero core size in experiments or simulations introduces OP-like corrections in the correlation function and structure factor.

The case with $n > d$ is unusual in that there are no topological defects, and it is not possible to describe the evolution of the system in terms of the annealing of defects. As a matter of fact, systems with $n > d$ need not exhibit dynamical scaling. Some specific results are available for $n = d + 1$, where the system is characterized by the presence of textures [52,53]. In general, systems with textures do not show single-length scaling. Dynamical scaling is restored in the $n \to \infty$ limit, where the correlation function exhibits a Gaussian decay [3]:

$$C(\vec{r}, t) = \exp\left(-\frac{r^2}{L^2}\right), \tag{1.173}$$

where $L(t) \sim t^{1/2}$. There are no general analytical results available for the correlation function of the n-component TDGL equation with $n > d$.

The results of OJK-OP and BPT have been understood to constitute a complete solution of the nonconserved ordering problem. However, the work of Blundell et al. [54] suggests that this is not the case. Generally, one tests for dynamical scaling by plotting $C(\vec{r}, t)$ versus r/L or $S(\vec{k}, t)L^{-d}$ versus kL at different times (see Figure 1.7) [55]. One also compares the analytical results with experimental or numerical results using similar plots. However, there is an arbitrariness in the definition of the characteristic length scale, which is defined as (say) the reciprocal of the first moment of the structure factor, or the distance over which the correlation function falls to half its maximum value. The problem with these definitions, while comparing different results, is that they already build in a high level of agreement on a scaling plot. Blundell et al. [54] have proposed a universal test of dynamical scaling, which does not use an internally defined length scale, but rather uses higher-order structure factors. On such a plot, there is a considerable difference between the OJK/BPT results and the corresponding numerical results. This suggests that our analytical understanding of nonconserved phase ordering may not be so good after all. Subsequently, Mazenko [57–59] showed that the OJK result is exact in the limit $d \to \infty$. There have been attempts to improve on the OJK result for the case of finite d, and these are discussed by Mazenko [60,61].

1.5 DOMAIN GROWTH IN SYSTEMS WITH CONSERVED KINETICS

Let us next consider systems with a conserved order parameter, for example, kinetics of phase separation of a binary (AB) mixture. A typical phase diagram for an AB mixture was shown in Figure 1.3. Though the Hamiltonian of the binary mixture is

the same as that for the ferromagnet, recall that the phase diagrams in Figures 1.2 and 1.3 are obtained in different ensembles.

In Figure 1.10, we show the evolution of a binary mixture after a quench from above the coexistence curve (homogeneous phase) to below the coexistence curve (segregated phase). The initially homogeneous system separates into A-rich and B-rich domains, denoted as black and white regions in Figure 1.10. In contrast with the nonconserved case, the evolution in this case must satisfy the constraint that numbers of A and B are constant, that is, the order parameter is conserved. In the corresponding kinetic Ising model in Section 1.3.3, recall that the conservation law was implemented via Kawasaki spin-exchange kinetics.

Experimentalists distinguish between shallow quenches (just below the coexistence curve) and deep quenches (far below the coexistence curve). For shallow quenches, in the region between the coexistence line and the spinodal lines in

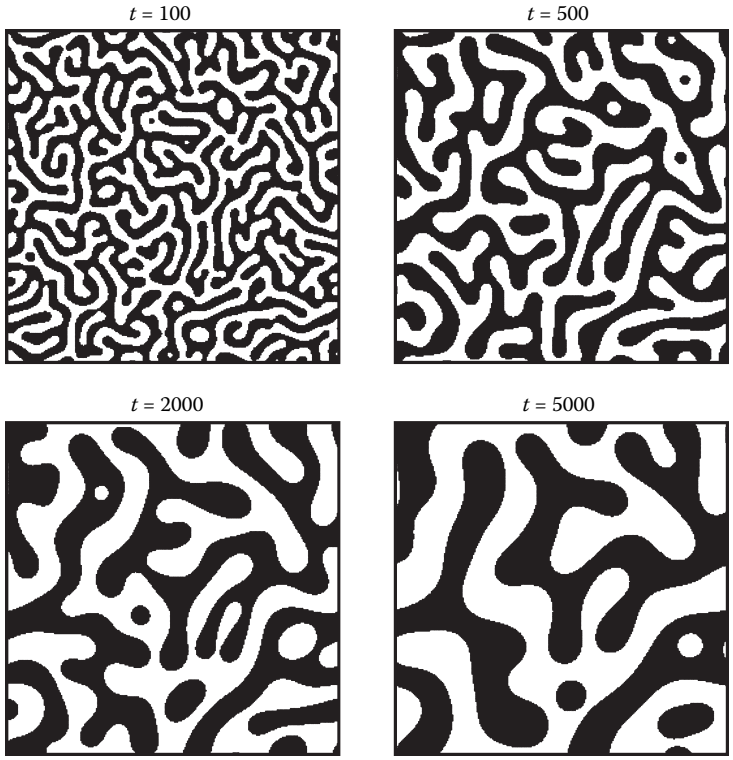

FIGURE 1.10 Evolution of a homogeneous binary (AB) mixture, which is quenched below the coexistence curve at time $t = 0$. These pictures were obtained from a numerical solution of the CHC equation 1.182 with $\epsilon = 0$. The discretization mesh sizes were $\Delta t = 0.01$ and $\Delta x = 1$, and the lattice size was 256^2. The random initial condition consisted of small-amplitude fluctuations about $\psi = 0$, corresponding with a mixture with equal amounts of A and B (critical composition). Regions with $\psi > 0$ (A-rich) and $\psi < 0$ (B-rich) are marked in black and white, respectively.

Figure 1.3, the homogeneous system is metastable and decomposes by the *nucleation and growth* of droplets. For deep quenches, into the region below the spinodal lines, the homogeneous system spontaneously decomposes into A-rich and B-rich regions, a process referred to as *spinodal decomposition*. However, there is no sharp physical distinction between the *nucleation and growth* and *spinodal decomposition* regions of the phase diagram [4]. This will be discussed at length in Chapter 2.

1.5.1 Segregation in Binary Alloys

First, we focus on the kinetics of phase separation in a binary mixture where hydrodynamic effects are not relevant, for example, binary alloys. In this case, the primary mechanism for phase separation is diffusion and aggregation. As in the nonconserved case, we introduce a space-time–dependent order parameter $\psi(\vec{r},t) = n^A(\vec{r},t) - n^B(\vec{r},t)$, where $n^\alpha(\vec{r},t)$ is the local density of species α. The evolution of ψ is described by the continuity equation:

$$\frac{\partial}{\partial t}\psi(\vec{r},t) = -\vec{\nabla}\cdot\vec{J}(\vec{r},t), \tag{1.174}$$

where $\vec{J}(\vec{r},t)$ denotes the current. Further, because the current is driven by concentration fluctuations, we expect

$$\vec{J}(\vec{r},t) = -D\vec{\nabla}\mu(\vec{r},t), \tag{1.175}$$

where D is the diffusion coefficient and $\mu(\vec{r},t)$ is the chemical potential. Finally, the chemical potential is determined as

$$\mu(\vec{r},t) = \frac{\delta F[\psi]}{\delta\psi}, \tag{1.176}$$

where F refers to the Helmholtz potential, which is the appropriate thermodynamic potential for the binary mixture. This is obtained from Equation 1.60 with $g(\psi)$ replaced by $f(\psi)$.

Combining Equations 1.174 through 1.176, we obtain the CH equation [62,63] for the phase separation of a binary mixture:

$$\frac{\partial}{\partial t}\psi(\vec{r},t) = D\nabla^2\left(\frac{\delta F[\psi]}{\delta\psi}\right). \tag{1.177}$$

In Section 1.3.3, we had derived this equation from the spin-exchange kinetic Ising model (cf. Equation 1.58). Notice that Equation 1.177 corresponds to the case of a constant diffusion coefficient. There have also been studies of systems where the diffusion coefficient depends on the local order parameter [64].

The effects of thermal fluctuations can be incorporated in the CH equation by including a noise term in the definition of the current in Equation 1.175 [65]. The resultant model is the Cahn–Hilliard–Cook (CHC) equation:

$$\frac{\partial}{\partial t}\psi(\vec{r},t) = \vec{\nabla}\cdot\left\{D\vec{\nabla}\left(\frac{\delta F[\psi]}{\delta\psi}\right) + \vec{\theta}(\vec{r},t)\right\}. \tag{1.178}$$

The vector noise satisfies the usual fluctuation–dissipation relation:

$$\begin{aligned} \overrightarrow{\vec{\theta}(\vec{r},t)} &= 0, \\ \overrightarrow{\theta_i(\vec{r}',t')\theta_j(\vec{r}'',t'')} &= 2Dk_BT\delta_{ij}\delta(\vec{r}'-\vec{r}'')\delta(t'-t''). \end{aligned} \tag{1.179}$$

Equations 1.178 and 1.179 are also referred to as *Model B* in the classification scheme of Hohenberg and Halperin [31].

For the ψ^4-form of the free-energy functional (Equation 1.63 without the magnetic field term), the CHC equation has the following form:

$$\frac{\partial}{\partial t}\psi(\vec{r},t) = \vec{\nabla}\cdot\left\{D\vec{\nabla}\left[-a(T_c-T)\psi + b\psi^3 - K\nabla^2\psi\right] + \vec{\theta}(\vec{r},t)\right\}. \tag{1.180}$$

In analogy with the TDGL equation (cf. Equation 1.64), we rescale variables as follows (for $T < T_c$):

$$\begin{aligned} \psi' &= \frac{\psi}{\psi_0}, \quad \psi_0 = \sqrt{\frac{a(T_c-T)}{b}}, \\ t' &= \frac{Da^2(T_c-T)^2}{K}\,t, \\ \vec{r}' &= \sqrt{\frac{a(T_c-T)}{K}}\,\vec{r}, \quad \xi_b = \sqrt{\frac{2K}{a(T_c-T)}}, \\ \vec{\theta}' &= \frac{\sqrt{bK}}{Da^2(T_c-T)^2}\,\vec{\theta}. \end{aligned} \tag{1.181}$$

We then drop primes to obtain the dimensionless CHC equation:

$$\frac{\partial}{\partial t}\psi(\vec{r},t) = \vec{\nabla}\cdot\left[\vec{\nabla}\left(-\psi+\psi^3-\nabla^2\psi\right) + \vec{\theta}(\vec{r},t)\right], \tag{1.182}$$

where

$$\begin{aligned} \overrightarrow{\vec{\theta}(\vec{r},t)} &= 0, \\ \overrightarrow{\theta_i(\vec{r}',t')\theta_j(\vec{r}'',t'')} &= 2\epsilon\delta_{ij}\delta(\vec{r}'-\vec{r}'')\delta(t'-t''), \\ \epsilon &= \frac{k_BTb\,[a(T_c-T)]^{(d-4)/2}}{K^{d/2}}. \end{aligned} \tag{1.183}$$

The evolution depicted in Figure 1.10 is obtained from a numerical solution of the dimensionless CHC equation with a random initial condition, which mimics the disordered state prior to the quench. Regions that are A-rich ($\psi = +1$) are marked black, and regions that are B-rich ($\psi = -1$) are not marked. The mixture has a critical composition with 50% A–50% B, that is, the average value of the order parameter

$\psi_0 = V^{-1} \int d\vec{r}\ \psi(\vec{r}, 0) = 0$. This composition is maintained during the evolution due to the conservation constraint. As in the case of the TDGL equation, thermal noise is asymptotically irrelevant for the CHC equation—the evolution shown in Figure 1.10 corresponds to the deterministic case with $\epsilon = 0$. In Figure 1.11, we show the evolution for an off-critical composition with 30% A and 70% B, that is, $\psi_0 = -0.4$. This composition still lies inside the spinodal curve in Figure 1.3, so the evolution corresponds to spinodal decomposition. However, the morphology is characterized by the growth of A-rich (minority phase) droplets in a B-rich (majority phase) background.

Before we proceed, it is relevant to discuss the applicability of the CHC model to real binary alloys. Typically, lattice parameter mismatches in alloys can set up large strain fields in the intermediate and late stages of phase separation [66–69] These strain fields drastically modify the results we quote below and must be accounted for in any realistic description of phase separation in alloys. Chapter 8 of this book addresses this problem in considerable detail.

In the absence of strain effects, the phase-separating system is characterized by a unique length scale, $L(t) \sim t^{1/3}$ in $d \geq 2$. This power-law behavior was first derived

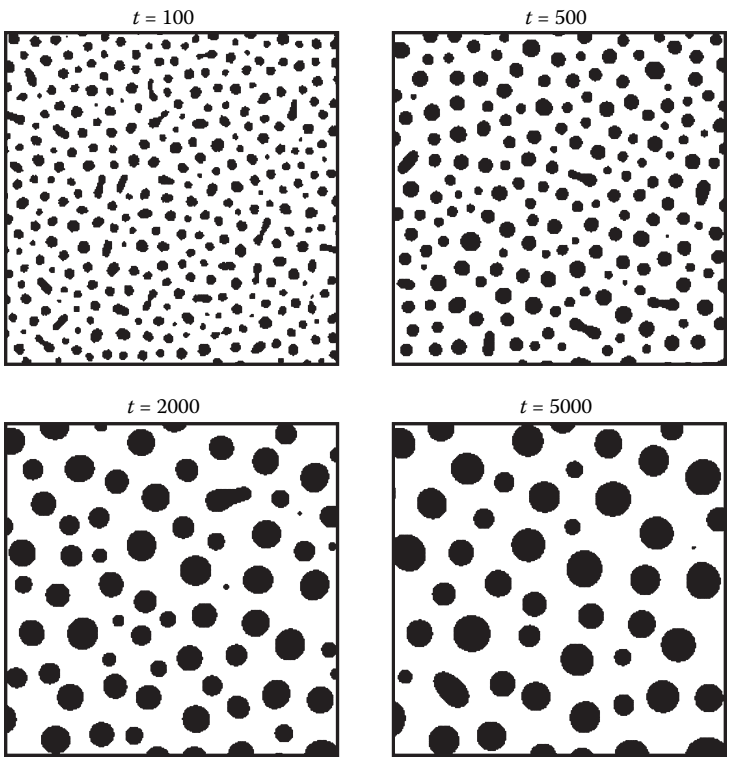

FIGURE 1.11 Analogous to Figure 1.10, but for the case of an off-critical binary mixture. The initial condition consisted of small-amplitude fluctuations about $\psi = -0.4$, corresponding to a mixture with 30% A and 70% B.

by Lifshitz and Slyozov (LS) [70] for extremely off-critical systems, where one of the components is present in a vanishing fraction, and the evolution proceeds via the nucleation and growth of minority droplets. Huse [71] demonstrated that the same law is applicable to spinodal decomposition, where there are approximately equal fractions of the two components, and the coarsening structure is bi-continuous. Typically, the chemical potential on the surface of a domain of size L is $\mu \sim \sigma/L$, where σ is the surface tension. The concentration current is obtained as $D|\vec{\nabla}\mu| \sim D\sigma/L^2$, where D is the diffusion constant. Therefore, the domain size grows as $dL/dt \sim D\sigma/L^2$, or $L(t) \sim (D\sigma t)^{1/3}$. In Figure 1.12, we show the domain growth law for the case with $\psi_0 = 0$ (shown in Figure 1.10)—the asymptotic growth law is seen to be consistent with the LS law.

As in the nonconserved case, the quantities that characterize the evolution morphology in Figures 1.10 and 1.11 are the correlation function and the structure factor. The existence of a characteristic length scale results in the dynamical scaling of these quantities. For the critical quench shown in Figure 1.10, we demonstrate the dynamical scaling of the correlation function and structure factor in Figure 1.13. The presence of interfacial defects results in a Porod tail for the scaled structure factor, $f(p) \sim p^{-(d+1)}$ as $p \to \infty$; and a singular short-distance behavior of the correlation function as in Equation 1.99. The structure factor also obeys the Tomita sum rule [41].

The above properties are common to the nonconserved and conserved cases. There are some additional features due to the conservation law. For example, the

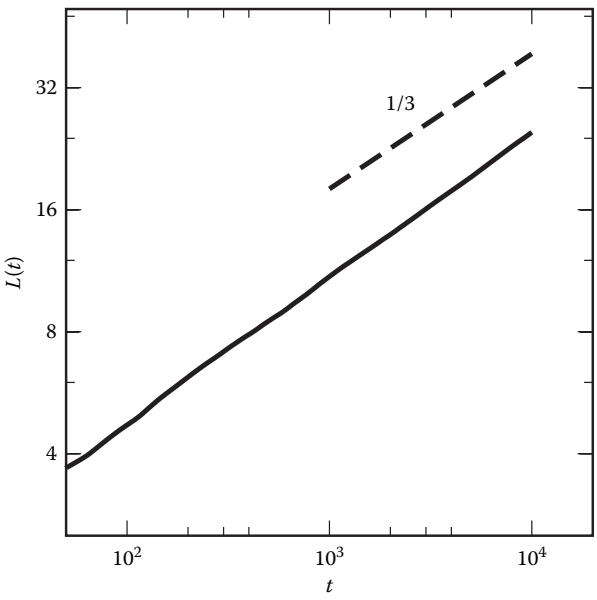

FIGURE 1.12 Domain growth law for the evolution depicted in Figure 1.10. The numerical data was obtained as an average over 10 independent runs for systems of size 512^2. The data is plotted on a log-log scale. The dashed line denotes the Lifshitz–Slyozov growth law, $L(t) \sim t^{1/3}$.

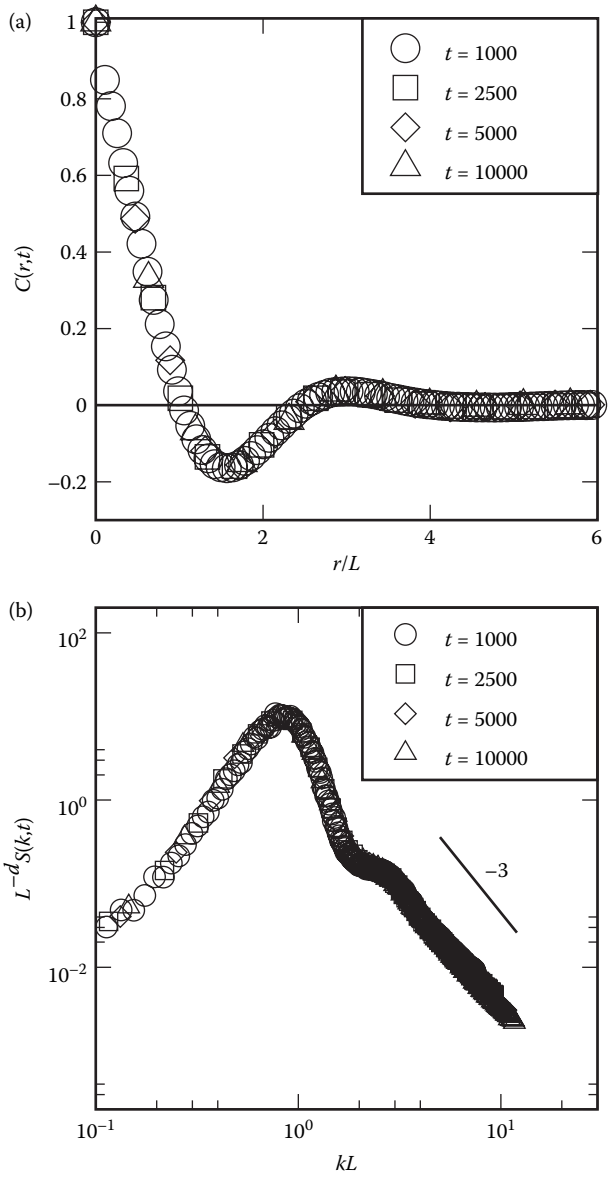

FIGURE 1.13 Analogous to Figure 1.7, but for the evolution depicted in Figure 1.10. The numerical data was obtained as an average over 10 independent runs for systems of size 512^2.

conservation constraint dictates the sum rule:

$$\int d\vec{r}\, C(\vec{r},t) = 0, \quad \text{or} \quad S(0,t) = 0. \tag{1.184}$$

Furthermore, the conservation law also fixes the $p \to 0$ behavior of the scaled structure factor as $f(p) \sim p^4$ [72,73].

Clearly, we have a good understanding of various general features of the morphology. There have also been extensive simulations of phase-separation kinetics, which have provided detailed results for the late-time behavior. These studies are based on *cell dynamical system* (CDS) models [49,50]; discrete simulations of the CHC equation [74]; and Monte Carlo (MC) simulations of the spin-exchange kinetic Ising model [75,76]. A detailed description of MC simulation techniques for domain growth problems is provided in Chapter 3. However, in spite of many attempts [77–79], there is still no comprehensive theory for the scaling form of the correlation function. A major analytical obstacle in this regard is the strongly correlated motion of interfaces, resulting from the conservation law. In particular, the *Gaussian closure* techniques introduced in Section 1.4.1, which involve linearization of the dynamical equations via a nonlinear transformation, have not worked well in the conserved case [82].

There have also been some studies of the case with conserved vector order parameter, that is, the conserved counterpart of Equation 1.164. In the case where topological defects are present ($n \leq d$), Puri et al. [83,84] demonstrated that Gaussian closure techniques work better than in the case with scalar order parameter. They used this approach to obtain approximate analytical results for the correlation functions of the conserved XY and Heisenberg models. The corresponding growth law is $L(t) \sim t^{1/4}$, which is slower than the LS-growth for the scalar case. In the limit $n \to \infty$, an important result is due to Coniglio and Zannetti [85], who showed that the structure factor exhibits *multiple-length* scaling rather than single-length scaling. However, Bray and Humayun [86] have demonstrated that multi-scaling is a singular property of the $n = \infty$ case.

1.5.2 Segregation in Binary Fluid Mixtures

1.5.2.1 Dimensional Form of Model H

Let us next consider the phase-separation kinetics of immiscible binary fluids [3–6]. In this case, the flow field enables advective transport of the segregating components. The appropriate equation for the order-parameter evolution is [31]

$$\frac{D\psi}{Dt} = \frac{\partial \psi}{\partial t} + \vec{v} \cdot \vec{\nabla}\psi = \vec{\nabla} \cdot \left(D\vec{\nabla}\mu + \vec{\theta} \right), \tag{1.185}$$

where $\vec{v}(\vec{r}, t)$ denotes the fluid velocity field. We assume that the fluid is incompressible (with constant density ρ). Recall that the density obeys the continuity equation:

$$\frac{\partial \rho}{\partial t} + \vec{\nabla} \cdot (\rho \vec{v}) = 0. \tag{1.186}$$

The requirement that ρ is constant imposes a constraint on the velocity field as $\vec{\nabla} \cdot \vec{v} = 0$.

The corresponding equation for the velocity field is the Navier–Stokes equation:

$$\rho \frac{D\vec{v}}{Dt} = \rho \left[\frac{\partial \vec{v}}{\partial t} + (\vec{v} \cdot \vec{\nabla})\vec{v} \right] = \eta \nabla^2 \vec{v} - \vec{\nabla} p - \psi \vec{\nabla} \mu + \vec{\zeta}, \tag{1.187}$$

where η is the viscosity, and p is the pressure. The additional term on the RHS, $-\psi\vec{\nabla}\mu$, describes the force exerted on the fluid by the segregating mixture.

The Gaussian white noise $\vec{\theta}$ in Equation 1.185 satisfies the fluctuation-dissipation relation (see Equation 1.179):

$$\begin{aligned} \overline{\vec{\theta}(\vec{r}, t)} &= 0, \\ \overline{\theta_i(\vec{r}', t')\theta_j(\vec{r}'', t'')} &= 2Dk_B T \delta_{ij} \delta(\vec{r}' - \vec{r}'') \delta(t' - t''). \end{aligned} \tag{1.188}$$

Equation 1.187 consists of three equations (for v_x, v_y, v_z) with noises $\zeta_x, \zeta_y, \zeta_z$. Each of these independent noises is obtained as

$$\zeta_i = \vec{\nabla} \cdot \vec{\sigma}, \tag{1.189}$$

where $\vec{\sigma}$ obeys the fluctuation-dissipation relation:

$$\begin{aligned} \overline{\vec{\sigma}(\vec{r}, t)} &= 0, \\ \overline{\sigma_i(\vec{r}', t')\sigma_j(\vec{r}'', t'')} &= 2\eta k_B T \delta_{ij} \delta(\vec{r}' - \vec{r}'') \delta(t' - t''). \end{aligned} \tag{1.190}$$

Our first task is to eliminate the pressure term in Equation 1.187 by using the incompressibility condition $\vec{\nabla} \cdot \vec{v} = 0$. We apply the operator $\vec{\nabla}\cdot$ to both sides of Equation 1.187 to obtain

$$\nabla^2 p = \vec{\nabla} \cdot \vec{F} = \vec{\nabla} \cdot \left[-\psi \vec{\nabla} \mu - \rho(\vec{v} \cdot \vec{\nabla})\vec{v} + \vec{\zeta} \right]. \tag{1.191}$$

In Fourier space, this equation has the solution

$$p(\vec{k}, t) = i \, \frac{\vec{k} \cdot \vec{F}(\vec{k}, t)}{k^2}. \tag{1.192}$$

We can replace $p(\vec{r}, t)$ [the inverse Fourier transform of $p(\vec{k}, t)$] in Equation 1.187 to obtain

$$\rho \frac{\partial}{\partial t} \vec{v}(\vec{r}, t) = \eta \nabla^2 \vec{v} + \left[-\psi \vec{\nabla} \mu - \rho(\vec{v} \cdot \vec{\nabla})\vec{v} + \vec{\zeta} \right]_\perp. \tag{1.193}$$

In Equation 1.193, we have introduced the following notation: $[\vec{F}(\vec{r}, t)]_\perp$ denotes the transverse part of the vector $\vec{F}(\vec{r}, t)$. In momentum space, this is computed as

$$[\vec{F}(\vec{k}, t)]_\perp = \vec{F}(\vec{k}, t) - \frac{\vec{k} \cdot \vec{F}(\vec{k}, t)}{k^2} \, \vec{k} = \vec{F}(\vec{k}, t) - \left[\hat{k} \cdot \vec{F}(\vec{k}, t) \right] \hat{k}. \tag{1.194}$$

Equations 1.185 and 1.193 are referred to as *Model H* in the classification scheme of Hohenberg and Halperin [31]. In analogy with Models A and B, we can rescale variables in Model H to obtain a dimensionless version. However, to clarify the domain growth laws in this model, it is convenient to work with the dimensional form.

1.5.2.2 Domain Growth Laws in Binary Fluids

To understand the domain growth laws, we consider the deterministic case with $T = 0$. In the initial stages, the dynamics of the velocity field is much faster than that of the order-parameter field, and we ignore the inertial terms in Equation 1.193. The resultant equation is solved for $\vec{v}$ (in Fourier space) as

$$\begin{aligned} v_i(\vec{k},t) &= T_{ij}(\vec{k})X_j(\vec{k},t) \\ &= \frac{1}{\eta k^2}\left(\delta_{ij} - \frac{k_i k_j}{k^2}\right) X_j(\vec{k},t), \\ \vec{X}(\vec{k},t) &= \int d\vec{r} e^{i\vec{k}\cdot\vec{r}} \left(-\psi\vec{\nabla}\mu\right). \end{aligned} \tag{1.195}$$

In Equation 1.195, repeated indices are summed over, and $T_{ij}(\vec{k})$ denotes the Oseen tensor in momentum space. In $d = 3$, the real-space Oseen tensor is

$$T_{ij}(\vec{r}) = \frac{1}{8\pi\eta r}\left(\delta_{ij} + \frac{r_i r_j}{r^2}\right). \tag{1.196}$$

As $\vec{\nabla}\cdot\vec{v} = 0$, we can rewrite Equation 1.185 as

$$\frac{\partial}{\partial t}\psi(\vec{r},t) = \vec{\nabla}\cdot\left(D\vec{\nabla}\mu - \psi\vec{v}\right), \tag{1.197}$$

where we have set $\vec{\theta} = 0$. Replacing the expression for the velocity from Equation 1.195 in Equation 1.197, we obtain the evolution equation

$$\frac{\partial}{\partial t}\psi(\vec{r},t) = D\nabla^2\mu + \nabla_i\left[\psi(\vec{r},t)\int d\vec{r}' T_{ij}(\vec{r}-\vec{r}')\psi(\vec{r}',t)\nabla'_j\mu(\vec{r}',t)\right]. \tag{1.198}$$

By partial integration, we can transform Equation 1.198 into a more symmetric form:

$$\frac{\partial}{\partial t}\psi(\vec{r},t) = D\nabla^2\mu - \left[\nabla_i\psi(\vec{r},t)\right]\int d\vec{r}' T_{ij}(\vec{r}-\vec{r}')\left[\nabla'_j\psi(\vec{r}',t)\right]\mu(\vec{r}',t) \tag{1.199}$$

where we have used the property

$$\nabla_i T_{ij}(\vec{r}-\vec{r}') = \nabla'_j T_{ij}(\vec{r}-\vec{r}') = 0. \tag{1.200}$$

Equation 1.198 or 1.199 can be used to understand domain growth laws for coarsening in binary fluids. At early times, growth is driven by diffusion, as in the

case of binary alloys. However, there is a crossover to a hydrodynamic growth regime, where material is rapidly transported along domain boundaries by advection [87,88]. Let us estimate the various terms in Equation 1.199. The term on the left-hand side (LHS) is estimated as

$$\frac{\partial \psi}{\partial t} \sim \frac{1}{L}\frac{dL}{dt}, \tag{1.201}$$

where $L(t)$ is the domain length scale. Next, consider the terms on the RHS. The diffusive term is of order $D\sigma/L^3$, where σ is the surface tension. (Recall that $\mu = \sigma/L$ on the surface of a domain with size L.) The advective term is of order $\sigma/(\eta L)$, where we have estimated the Oseen tensor as $T \sim 1/(\eta L)$ in $d = 3$. Thus, the diffusive term is dominant when

$$\frac{D\sigma}{L^3} \gg \frac{\sigma}{\eta L}, \tag{1.202}$$

or $L \ll (D\eta)^{1/2}$. The growth law in the diffusive regime is the usual LS law, $L(t) \sim (D\sigma t)^{1/3}$. At later times, the advective term is dominant, yielding the following growth law for the so-called *viscous hydrodynamic* regime:

$$L(t) \sim \frac{\sigma t}{\eta}. \tag{1.203}$$

At even later times, the approximation of neglecting the inertial terms in Equation 1.193 is no longer valid [88]. To understand this, let us estimate the terms in Equation 1.193, which we repeat here for ease of reference:

$$\rho\frac{\partial \vec{v}}{\partial t} + [\rho(\vec{v}\cdot\vec{\nabla})\vec{v}]_\perp = \eta\nabla^2\vec{v} - \left[\psi\vec{\nabla}\mu\right]_\perp, \tag{1.204}$$

where we have set $\vec{\zeta} = 0$. The fluid velocity scale is estimated as L/t. Then, the first term on the LHS is of order $\rho L/t^2$, and the second (nonlinear) term is also of the same order. The viscous term on the RHS is of order $\eta/(Lt)$, and the force term is of order σ/L^2. The terms on the LHS become comparable with those on the RHS at length scales of order $\eta^2/(\rho\sigma)$. The asymptotic growth law in the *inertial hydrodynamic* regime is then obtained from

$$\frac{\rho L}{t^2} \sim \frac{\sigma}{L^2}, \tag{1.205}$$

as

$$L(t) \sim \left(\frac{\sigma t^2}{\rho}\right)^{1/3}. \tag{1.206}$$

The growth laws for the different regimes are summarized as follows:

$$\begin{aligned} L(t) &\sim (D\sigma t)^{1/3}, \quad L \ll (D\eta)^{1/2}, \quad (\textit{diffusive regime}) \\ &\sim \frac{\sigma t}{\eta}, \quad (D\eta)^{1/2} \ll L \ll \frac{\eta^2}{\rho\sigma}, \quad (\textit{viscous hydrodynamic regime}) \\ &\sim \left(\frac{\sigma t^2}{\rho}\right)^{1/3}, \quad \frac{\eta^2}{\rho\sigma} \ll L, \quad (\textit{inertial hydrodynamic regime}) \end{aligned} \tag{1.207}$$

Grant and Elder [89] have argued that scaling requires that the asymptotic growth exponent $\phi \leq 1/2$. Otherwise, the system enters a turbulent regime in which it undergoes remixing. Alternatively, they suggest that a faster growth law than $L(t) \sim t^{1/2}$ can be sustained if the system does not exhibit dynamical scaling. However, the Grant–Elder arguments have been criticized by Kendon et al. [90], whose lattice-Boltzmann simulations support the inertial hydrodynamic growth law, $L(t) \sim t^{2/3}$. (A detailed description of the lattice-Boltzmann approach to study the phase separation of fluids is provided in Chapter 4.)

We should also stress that domain connectivity plays a crucial role in enabling hydrodynamic transport. In highly off-critical quenches, the morphology consists of droplets of the minority phase in a matrix of the majority phase (see Figure 1.11). Then, the hydrodynamic mechanism is disabled and domain growth is analogous to that for binary alloys. Furthermore, thermal fluctuations can drive the Brownian motion and coalescence of droplets. This also gives rise to a LS-like growth law, $L(t) \sim (k_B T t/\eta)^{1/3}$ [87], though the physical mechanism is quite different.

Finally, we should remark on the morphology, as characterized by the correlation function or the structure factor. These quantities and the domain growth laws have been investigated in many numerical studies, for example, CDS simulations [91–94]; molecular dynamics (MD) studies [95,96]; lattice-Boltzmann simulations [90,97,98], etc. As regards analytical results, the general morphological features (Porod's law, Tomita sum rule, etc.) discussed in Section 1.4.1 arise in the current context also. However, as in the case of binary alloys, there is no satisfactory theory for the scaling form of the correlation function. This remains one of the major unsolved problems in the field of phase-ordering kinetics.

1.6 SUMMARY AND DISCUSSION

Let us conclude this chapter with a summary and discussion. We have presented a broad overview of the *kinetics of phase transitions*. There are two prototypical problems in this area: (a) the ordering of a ferromagnet, which is an example of the case with nonconserved order parameter; and (b) the phase separation of a binary mixture, which is an example of the case with conserved order parameter. One is interested in the evolution of a thermodynamically unstable disordered or homogeneous state. This

evolution is characterized by the emergence and growth of domains that are enriched in different components of the mixture.

We have a good understanding of the morphologies and growth laws that characterize domain-growth kinetics. The domain size $L(t)$ usually grows as a power-law in time, $L(t) \sim t^{\phi}$, where the exponent ϕ depends on (a) the nature of conservation laws, (b) the defects that drive the ordering process, and (c) the relevance of flow fields. The morphology is quantitatively characterized by the correlation function or its Fourier transform, the structure factor. There is a good theoretical understanding of the correlation function for nonconserved dynamics with both scalar and vector order parameters. Unfortunately, our understanding of the conserved problem is not so good. Thus, we know the various limiting behaviors of the correlation function or structure factor. However, the overall functional form is not well understood, and this remains one of the outstanding problems in this area.

We should stress that the concepts and paradigms discussed here have been applied in a broad variety of physical problems. The examples used in this chapter are primarily drawn from metallurgy and materials science. However, the phenomena of phase separation, clustering, and aggregation are ubiquitous in nature.

The subsequent chapters of this book will discuss different aspects of the kinetics of phase transitions. All the chapters are written in a pedagogical manner and will be accessible to an advanced undergraduate student. At this stage, it is useful to provide a brief overview of these chapters. We have mentioned earlier that the distinction between *spinodal decomposition* and *nucleation and growth* is not as sharp as the phase diagram in Figure 1.3 would suggest. This issue is discussed in detail by Binder in Chapter 2. Chapters 3 and 4 are dedicated to a discussion of simulation techniques in this area. In Chapter 3, Barkema describes Monte Carlo simulations of the kinetic Ising models introduced in Section 1.3. In Chapter 4, Gonnella and Yeomans discuss lattice Boltzmann simulations, which have proved very useful in understanding the late stages of phase separation in fluid mixtures (cf. Section 1.5.2). Numerical simulations have played a crucial role in developing our understanding of domain growth problems. The methodology described in Chapters 3 and 4 will prove very useful for a researcher entering this area.

In Chapter 5, Zannetti discusses *slow relaxation* and *aging* in phase-ordering systems. These phenomena are well known in the context of structural glasses and spin glasses. Recent studies indicate that these concepts are also highly relevant in domain growth problems—Zannetti provides an overview of these studies.

Recent interest in this area has focused on incorporating various experimentally relevant features in studies of phase-ordering systems. In this context, Chapter 6 (by Khanna, Agnihotri, and Sharma) discusses the *kinetics of dewetting* of liquid films on surfaces. In Chapter 7, Ohta reviews studies of phase separation in diblock copolymers. In these systems, the polymers A and B (which repel each other) are jointed, so that the system can only undergo segregation on microscales. Finally, in Chapter 8 (written by Onuki, Minami, and Furukawa), there is a detailed discussion of phase separation in solids. In Section 1.5.1, we had emphasized that strain fields play an important role in the segregation kinetics of alloys. Onuki et al. discuss how elastic fields can be incorporated into the Ginzburg–Landau description of solid mixtures.

ACKNOWLEDGMENTS

The author's understanding of the problems discussed here has grown through many fruitful collaborations. He would like to thank his research collaborators for many stimulating interactions and inputs. He is also grateful to Anupam Mukherjee for assistance in preparing the figures.

REFERENCES

1. Stanley, H.E., *Introduction to Phase Transitions and Critical Phenomena*, Oxford University Press, Oxford, 1971.
2. *Phase Transitions and Critical Phenomena*, Domb, C. and Lebowitz, J.L., Eds., Academic Press, London.
3. Bray, A.J., Theory of phase ordering kinetics, *Adv. Phys.*, 43, 357, 1994.
4. Binder, K. and Fratzl, P., Spinodal decomposition, in *Materials Science and Technology* Vol. 5, Kostorz, G., Ed., Wiley-VCH, Weinheim, 2001, chap. 6.
5. Onuki, A., *Phase Transition Dynamics*, Cambridge University Press, Cambridge, 2002.
6. Dattagupta, S. and Puri, S., *Dissipative Phenomena in Condensed Matter Physics*, Springer-Verlag, Heidelberg.
7. Plischke, M. and Bergersen, B., *Equilibrium Statistical Physics*, Second Edition, World Scientific, Singapore, 1994.
8. Glauber, R.J., Time-dependent statistics of the Ising model, *J. Math. Phys.*, 4, 294, 1963.
9. Kawasaki, K., Kinetics of Ising models, in *Phase Transitions and Critical Phenomena*, Vol. 2, Domb, C. and Green, M.S., Eds., Academic Press, London, 1972, 443.
10. Kawasaki, K., Diffusion constants near the critical point for time-dependent Ising models. I, *Phys. Rev.*, 145, 224, 1966.
11. Van Kampen, N.G., *Stochastic Processes in Physics and Chemistry*, North-Holland, Amsterdam, 1981.
12. Suzuki, M. and Kubo, R., Dynamics of the Ising model near the critical point. I, *J. Phys. Soc. Jpn.*, 24, 51, 1968.
13. Binder, K., Kinetic Ising model study of phase separation in binary alloys, *Z. Phys.*, 267, 313, 1974.
14. Binder, K., Theory for the dynamics of clusters. II. Critical diffusion in binary systems and the kinetics of phase separation, *Phys. Rev. B*, 15, 4425, 1977.
15. Gouyet, J.-F., Atomic mobility and spinodal-decomposition dynamics in lattice gases. Simple discrete models, *Europhys. Lett.*, 21, 335, 1993.
16. Gouyet, J.-F., Generalized Allen–Cahn equations to describe far-from-equilibrium order–disorder dynamics, *Phys. Rev. E*, 51, 1695, 1995.
17. Plapp, M. and Gouyet, J.-F., Dendritic growth in a mean-field lattice gas model, *Phys. Rev. E*, 55, 45, 1997.
18. Puri, S., Dynamics of vacancy-mediated phase separation, *Phys. Rev. E*, 55, 1752, 1997.
19. Puri, S. and Sharma, R., Phase ordering dynamics in binary mixtures with annealed vacancies, *Phys. Rev. E*, 57, 1873, 1998.
20. Landau, L.D. and Lifshitz, E.M., *Statistical Physics*, Pergamon Press, Oxford, 1980.
21. Huang, K., *Statistical Mechanics*, Second Edition, Wiley, New York, 1987.
22. Manning, J.R., *Diffusion Kinetics for Atoms in Crystals*, Van Nostrand, Princeton, 1968.
23. Flynn, C.P., *Point Defects and Diffusion*, Clarendon, Oxford, 1972.
24. Yaldram, K. and Binder, K., Spinodal decomposition of a two-dimensional model alloy with mobile vacancies, *Acta Metall.*, 39, 707, 1991.

25. Yaldram, K. and Binder, K., Monte Carlo simulation of phase separation and clustering in the ABV model, *J. Stat. Phys.*, 62, 161, 1991.
26. Tafa, K., Puri, S., and Kumar, D., Kinetics of domain growth in systems with local barriers, *Phys. Rev. E*, 63, 046115, 2001.
27. Tafa, K., Puri, S., and Kumar, D., Kinetics of phase separation in ternary mixtures, *Phys. Rev. E*, 64, 056139, 2001.
28. Bray, A.J., Comment on "Critical dynamics and global conservation laws," *Phys. Rev. Lett.*, 66, 2048, 1991.
29. Annett, J.F. and Banavar, J.R., Critical dynamics, spinodal decomposition, and conservation laws, *Phys. Rev. Lett.*, 68, 2941, 1992.
30. Phani, M.K., Lebowitz, J.L., Kalos, M.H., and Penrose, O., Kinetics of an order-disorder transition, *Phys. Rev. Lett.*, 45, 366, 1980.
31. Hohenberg, P.C. and Halperin, B.I., Theory of dynamic critical phenomena, *Rev. Mod. Phys.*, 49, 435, 1977.
32. Allen, S.M. and Cahn, J.W., A microscopic theory for antiphase boundary motion and its application to antiphase domain coarsening, *Acta Metall.*, 27, 1085, 1979.
33. Puri, S. and Oono, Y., Effect of noise on spinodal decomposition, *J. Phys. A*, 21, L755, 1988.
34. Bray, A.J., Exact renormalization-group results for domain-growth scaling in spinodal decomposition, *Phys. Rev. Lett.*, 62, 2841, 1989.
35. Bray, A.J., Renormalization-group approach to domain-growth scaling, *Phys. Rev. B*, 41, 6724, 1990.
36. Binder, K. and Stauffer, D., Theory for the slowing down of the relaxation and spinodal decomposition of binary mixtures, *Phys. Rev. Lett.*, 33, 1006, 1974.
37. Nagai, T. and Kawasaki, K., Statistical dynamics of interacting kinks II, *Physica A*, 134, 483, 1986.
38. Gradshteyn, I.S. and Ryzhik, I.M., *Table of Integrals, Series, and Products*, Academic Press, London, 1994.
39. Porod, G., in *Small-Angle X-Ray Scattering*, Glatter, O. and Kratky, O., Eds., Academic Press, New York, 1982, 42.
40. Ohta, T., Jasnow, D., and Kawasaki, K., Universal scaling in the motion of random interfaces, *Phys. Rev. Lett.*, 49, 1223, 1982.
41. Tomita, H., Sum rules for small angle scattering by random interface, *Prog. Theor. Phys.*, 72, 656, 1984.
42. Tomita, H., Statistical properties of random interface system, *Prog. Theor. Phys.*, 75, 482, 1986.
43. Oono, Y. and Puri, S., Large wave number features of form factors for phase transition kinetics, *Mod. Phys. Lett. B*, 2, 861, 1988.
44. Kawasaki, K., Yalabik, M.C., and Gunton, J.D., Growth of fluctuations in quenched time-dependent Ginzburg–Landau model systems, *Phys. Rev. A*, 17, 455, 1978.
45. Suzuki, M., Scaling theory of non-equilibrium systems near the instability point. I. General aspects of transient phenomena, *Prog. Theor. Phys.*, 56, 77, 1976.
46. Suzuki, M., Scaling theory of non-equilibrium systems near the instability point. II. Anomalous fluctuation theorems in the extensive region, *Prog. Theor. Phys.*, 56, 477, 1976.
47. Bray, A.J. and Puri, S., Asymptotic structure factor and power-law tails for phase ordering in systems with continuous symmetry, *Phys. Rev. Lett.*, 67, 2670, 1991.
48. Toyoki, H., Structure factors of vector-order-parameter systems containing random topological defects, *Phys. Rev. B*, 45, 1965, 1992.

49. Bray, A.J. and Humayun, K., Universal amplitudes of power-law tails in the asymptotic structure factor of systems with topological defects, *Phys. Rev. E*, 47, R9, 1993.
50. Puri, S. and Roland, C., Approximate solutions of the two-component Ginzburg–Landau equation, *Phys. Lett. A*, 151, 500, 1990.
51. Pargellis, A.N., Finn, P., Goodby, J.W., Panizza, P., Yurke, B., and Cladis, P.E., Defect dynamics and coarsening dynamics in Smectic-C films, *Phys. Rev. A*, 46, 7765, 1992.
52. Newman, T.J., Bray, A.J., and Moore, M.A., Growth of order in vector spin systems and self-organized criticality, *Phys. Rev. B*, 42, 4514, 1990.
53. Zapotocky, M. and Zakrzewski, W., Kinetics of phase ordering with topological textures, *Phys. Rev. E*, 51, R5189, 1995.
54. Blundell, R.E., Bray, A.J., and Sattler, S., Absolute test for theories of phase-ordering dynamics, *Phys. Rev. E*, 48, 2476, 1993.
55. Oono, Y. and Puri, S., Computationally efficient modeling of ordering of quenched phases, *Phys. Rev. Lett.*, 58, 836, 1987.
56. Puri, S. and Oono, Y., Study of phase-separation dynamics by use of cell dynamical systems. II. Two-dimensional results, *Phys. Rev. A*, 38, 1542, 1988.
57. Mazenko, G.F., Theory of unstable thermodynamic systems, *Phys. Rev. Lett.*, 63, 1605, 1989.
58. Mazenko, G.F., Theory of unstable growth, *Phys. Rev. B*, 42, 4487, 1990.
59. Mazenko, G.F., Theory of unstable growth. II. Conserved order parameter, *Phys. Rev. B*, 43, 5747, 1991.
60. Mazenko, G.F., Perturbation expansion in phase-ordering kinetics: I. Scalar order parameter, *Phys. Rev. E*, 58, 1543, 1998.
61. Mazenko, G.F., Perturbation expansion in phase-ordering kinetics. II. n-vector model, *Phys. Rev. E*, 61, 1088, 2000.
62. Cahn, J.W. and Hilliard, J.E., Free energy of a nonuniform system. I. Interfacial free energy, *J. Chem. Phys.*, 28, 258, 1958.
63. Cahn, J.W. and Hilliard, J.E., Free energy of a nonuniform system. III. Nucleation in a two-component incompressible fluid, *J. Chem. Phys.*, 31, 688, 1959.
64. Puri, S., Bray, A.J., and Lebowitz, J.L., Segregation dynamics in systems with order-parameter dependent mobilities, *Phys. Rev. E*, 56, 758, 1997.
65. Cook, H.E., Brownian motion in spinodal decomposition, *Acta Metall.*, 18, 297, 1970.
66. Nishimori, H. and Onuki, A., Pattern formation in phase-separating alloys with cubic symmetry, *Phys. Rev. B*, 42, 980, 1990.
67. Onuki, A. and Nishimori, H., Anomalously slow domain growth due to a modulus inhomogeneity in phase-separating alloys, *Phys. Rev. B*, 43, 13649, 1991.
68. Langmayr, F., Fratzl, P., Vogl, G., and Miekeley, W., Crossover from omega-phase to alpha-phase precipitation in bcc Ti-Mo, *Phys. Rev. B*, 49, 11759, 1994.
69. Fratzl, P., Penrose, O., and Lebowitz, J.L., Modeling of phase separation in alloys with coherent elastic misfit, *J. Stat. Phys.*, 95, 1429, 1999.
70. Lifshitz, I.M. and Slyozov, V.V., The kinetics of precipitation from supersaturated solid solutions, *J. Phys. Chem. Solids*, 19, 35, 1961.
71. Huse, D.A., Corrections to late-stage behavior in spinodal decomposition: Lifshitz–Slyozov scaling and Monte Carlo simulations, *Phys. Rev. B*, 34, 7845, 1986.
72. Yeung, C., Scaling and the small-wave-vector limit of the form factor in phase-ordering dynamics, *Phys. Rev. Lett.*, 61, 1135, 1988.
73. Furukawa, H., Numerical study of multitime scaling in a solid system undergoing phase separation, *Phys. Rev. B*, 40, 2341, 1989.
74. Rogers, T.M., Elder, K.R., and Desai, R.C., Numerical study of the late stages of spinodal decomposition, *Phys. Rev. B*, 37, 9638, 1988.

75. Amar, J., Sullivan, F., and Mountain, R.D., Monte Carlo study of growth in the two-dimensional spin-exchange kinetic Ising model, *Phys. Rev. B*, 37, 196, 1988.
76. Marko, J.F. and Barkema, G.T., Phase ordering in the Ising model with conserved spin, *Phys. Rev. E*, 52, 2522, 1995.
77. Ohta, T. and Nozaki, H., Scaled correlation function in the late stage of spinodal decomposition, in *Space-Time Organization in Macromolecular Fluids*, Tanaka, F., Doi, M., and Ohta, T., Eds., Springer-Verlag, Berlin, 1989, 51.
78. Tomita, H., A new phenomenological equation of the interface dynamics, *Prog. Theor. Phys.*, 90, 521, 1993.
79. Mazenko, G.F., Growth kinetics for a system with a conserved order parameter, *Phys. Rev. E*, 50, 3485, 1994.
80. Mazenko, G.F. and Wickham, R., Growth kinetics for a system with a conserved order parameter: Off-critical quenches, *Phys. Rev. E*, 51, 2886, 1995.
81. Mazenko, G.F., Spinodal decomposition and the Tomita sum rule, *Phys. Rev. E*, 62, 5967, 2000.
82. Yeung, C., Oono, Y., and Shinozaki, A., Possibilities and limitations of Gaussian-closure approximations for phase-ordering dynamics, *Phys. Rev. E*, 49, 2693, 1994.
83. Puri, S., Bray, A.J., and Rojas, F., Ordering kinetics of conserved XY models, *Phys. Rev. E*, 52, 4699, 1995.
84. Rojas, F., Puri, S., and Bray, A.J., Kinetics of phase ordering in the O(n) model with a conserved order parameter, *J. Phys. A*, 34, 3985, 2001.
85. Coniglio, A. and Zannetti, M., Multiscaling in growth kinetics, *Europhys. Lett.*, 10, 575, 1989.
86. Bray, A.J. and Humayun, K., Scaling and multiscaling in the ordering kinetics of a conserved order parameter, *Phys. Rev. Lett.*, 68, 1559, 1992.
87. Siggia, E.D., Late stages of spinodal decomposition in binary mixtures, *Phys. Rev. A*, 20, 595, 1979.
88. Furukawa, H., Effect of inertia on droplet growth in a fluid, *Phys. Rev. A*, 31, 1103, 1985.
89. Grant, M. and Elder, K.R., Spinodal decomposition in fluids, *Phys. Rev. Lett.*, 82, 14, 1999.
90. Kendon, V.M., Desplat, J.-C., Bladon, P., and Cates, M.E., 3D spinodal decomposition in the inertial regime, *Phys. Rev. Lett.*, 83, 576, 1999.
91. Koga, T. and Kawasaki, K., Spinodal decomposition in binary fluids: Effects of hydrodynamic interactions, *Phys. Rev. A*, 44, R817, 1991.
92. Puri, S. and Dünweg, B., Temporally linear domain growth in the segregation of binary fluids, *Phys. Rev. A*, 45, R6977, 1992.
93. Shinozaki, A. and Oono, Y., Asymptotic form factor for spinodal decomposition in three-space, *Phys. Rev. Lett.*, 66, 173, 1991.
94. Shinozaki, A. and Oono, Y., Spinodal decomposition in 3-space, *Phys. Rev. E*, 48, 2622, 1993.
95. Laradji, M., Toxvaerd, S., and Mouritsen, O.G., Molecular dynamics simulation of spinodal decomposition in three-dimensional binary fluids, *Phys. Rev. Lett.*, 77, 2253, 1996.
96. Bastea, S. and Lebowitz, J.L., Spinodal decomposition in binary gases, *Phys. Rev. Lett.*, 78, 3499, 1997.
97. Higuera, F.J., Succi, S., and Benzi, R., Lattice gas dynamics with enhanced collisions, *Europhys. Lett.*, 9, 345, 1989.
98. Swift, M.R., Orlandini, E., Osborn, W.R., and Yeomans, J., Lattice Boltzmann simulations of liquid-gas and binary fluid systems, *Phys. Rev. E*, 54, 5041, 1996.